Optimisation of heat recovery from low-enthalpy aquifers with geological uncertainty using surrogate response surfaces and simple search algorithms

Babaei, Masoud; Norouzi, Amir Mohammad; Nick, Hamidreza M.; Gluyas, Jon

DOI
10.1016/j.seta.2021.101754

Publication date
2022

Document Version
Final published version

Published in
Sustainable Energy Technologies and Assessments

Citation (APA)
Babaei, M., Norouzi, A. M., Nick, H. M., & Gluyas, J. (2022). Optimisation of heat recovery from low-enthalpy aquifers with geological uncertainty using surrogate response surfaces and simple search algorithms. *Sustainable Energy Technologies and Assessments*, *49*, 1-19. Article 101754. https://doi.org/10.1016/j.seta.2021.101754

Sustainable Energy Technologies and Assessments 49 (2022) 101754

Contents lists available at ScienceDirect

Sustainable Energy Technologies and Assessments

journal homepage: www.elsevier.com/locate/seta

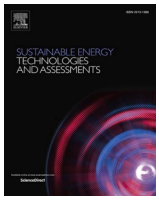

Optimisation of heat recovery from low-enthalpy aquifers with geological uncertainty using surrogate response surfaces and simple search algorithms

Masoud Babaei [a,*], Amir Mohammad Norouzi [a], Hamidreza M. Nick [b,c], Jon Gluyas [d]

[a] The University of Manchester, Department of Chemical Engineering and Analytical Science, Manchester, UK
[b] The Danish Hydrocarbon Research and Technology Centre, Technical University of Denmark, Lyngby, Denmark
[c] Department of Geoscience & Engineering, Delft University of Technology, Delft, Netherlands
[d] Department of Earth Sciences, Durham University, Durham, UK

ARTICLE INFO

Keywords:
Doublets
Well spacing
Low-enthalpy geothermal systems
Optimisation
Coefficient of performance

ABSTRACT

Optimisation of doublet well spacing in low-enthalpy geothermal systems is addressed by defining a novel objective function that is based on the Coefficient of Performance (CoP) and energy sweep efficiency. The definition of objective function that separates performance-based criteria from economic factors, allows us to better observe the effects of heterogeneity on optimisation. A checkerboard pattern of two doublets (two injection wells diagonally placed and two production wells diagonally placed over corners of a rectangle) is considered for a range of homogeneous to heterogeneous (spatially correlated and fluvial) synthetic low enthalpy reservoirs. Optimal length and width of this rectangle are sought in order to (a) maximise heat recovery from a conventionally-chosen licence area around the rectangular domain, (b) minimise heat recovery from outside this licence area, and (c) maximise CoP. We define fixed (15 years and 30 years) and varying life times of operation (between 15 and 30 years). For optimisation, in addition to a simple-search procedure of optimisation across a mesh of simulation nodes, we also utilise a surrogate response surface model to computationally solve the optimisation problem. Our results consistently show that for a fixed life time of 15 years and a discharge rate of 250 m^3/hr, 400 m is the optimal well/doublet spacing. Increasing the life time and the discharge rate will increase the optimal well/doublet spacing. The results show while CoP is sensitive to the heterogeneity, adding energy sweep to the objective function makes the distances found for the homogeneous cases also consistent solutions for the heterogeneous cases.

1. Introduction

1.1. Optimization of geothermal heat recovery

Optimization of geothermal doublet systems in terms of their spacing in heterogeneous aquifers has only been focused on recent studies [1,2]. In fact, in the review of Pandey et al. [3] on the geothermal reservoir modeling, there is no mention of optimisation of doublet systems. There are only few publications that studied doublet spacing optimization [4–11]. An early work by Sauty *et al.* [4], focused on lifetime optimization of doublets for the Parisian Basin Dogger by optimizing well spacing. Tselepidou and Katsifarakis [5] examined optimization of low enthalpy geothermal aquifer by accounting for the costs of annual pumping and amortization of the pipe network carrying the hot water from the wells to a water tank. Smit *et al.* [6] used gradient-based optimization for determining the best doublet spacing to maximise the Net Present Value (NPV) of doublets. While the authors considered heterogeneity of the system, the use of gradient-based optimization means that certain gradients must be calculated numerically (and iteratively) which can be a computationally prohibitive process. Ansari *et al.* [7] used Particle Swarm Optimization to select locations for 4 production and 4 re-injection geothermal wells out of a set of 11 existing abandoned wells in the US Gulf Coast. Kong *et al.* [8] used homogeneous geothermal reservoirs for doublet placement optimization. The authors used an economic analysis to define the objective function as the cost of reservoir exploitation (made up of the cost of electricity due to hydraulic head drawdown in the production well and the cost of thermal breakthrough). The model of the geothermal system employed was homogeneous and as such it was unrealistic. Jiang *et al.* [9] focused on doublet spacing optimization for low enthalpy geothermal systems accounting

* Corresponding author.
E-mail address: masoud.babaei@manchester.ac.uk (M. Babaei).

https://doi.org/10.1016/j.seta.2021.101754
Received 9 June 2021; Received in revised form 14 September 2021; Accepted 6 November 2021
Available online 19 November 2021

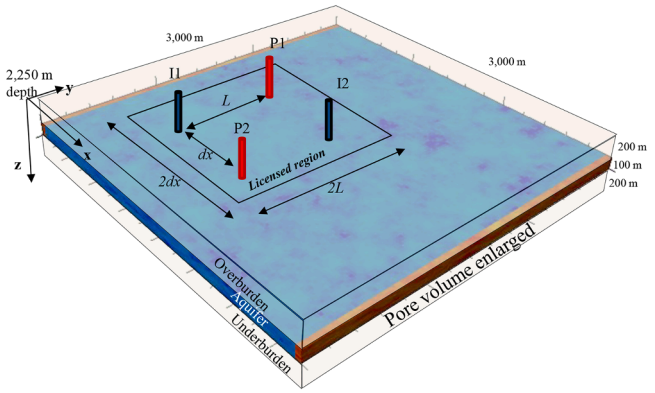

Fig. 1. The doublets configuration and the license-boundary control region of the subsurface system used in this study.

Table 1
The statistical properties of the homogeneous case and the heterogeneous cases used in this study.

Case	Mean (ϕ), mean (K[mD])	Min (ϕ), min (K[mD])	Max(ϕ), max (K[mD])	Std (ϕ), std (K[mD])
Homogeneous	0.15, 139.46	0.15, 139.46	0.15, 139.46	0, 0
Het. case 1	0.17, 613.4	0.01, 6.5×10^{-4}	0.34, 4,454	0.04, 667
Het. case 2	0.17, 606.2	0.01, 6.5×10^{-4}	0.35, 4,909	0.04, 658
Het. case 3	0.17, 605.2	0.01, 6.5×10^{-4}	0.34, 4,445	0.04, 655
Het. case 4	0.17, 607.2	0.01, 7.5×10^{-4}	0.34, 4,743	0.04, 661

for density-driven flow in confined aquifers. The authors found that depending on the regimes of flow and heat transport (free/forced/mixed convection and conduction), the operator can choose an optimum configuration (depth-wise and side-wise) for the doublets. Nonetheless, the results are derived only for homogeneous aquifers.

Willems and Nick [10] considered a large-scale numerical simulation-based planning to exploit Hot Sedimentary Aquifer (HSA) from the West Netherlands Basin. Various data were combined from different sources. The projection of heat recovery from a currently practiced scenario on a large geothermal aquifer in the Netherlands was shown to be very inefficient by the authors. In fact, the authors demonstrated that only 1% of the recoverable heat will be recovered if a currently and conventionally applied "first-come, first-served" based operation is implemented for geothermal energy exploitation. Therefore a "master plan" is required to design optimum well placement in doublet systems. A recent work by Liu et al. [11] proposed a new well pattern of cluster-layout and examined its performance in heterogeneous porous geothermal reservoir models based on the Dezhou geothermal field, China. The authors concluded that the proposed cluster-layout is an efficient pattern for maximising heat recovery, and the heat recovery is susceptible to inherent heterogeneity of the geothermal fields. However, the authors did not consider the well/doublet spacing, rather their focus was on well patterns. Heterogeneity has been considered in optimising geothermal heat extraction by recent studies of [1,2]. Schulte *et al.* [1] considered optimization of geothermal heat extraction using multi-objective particle swarm optimization. The authors used a subsection of Watt Field. The focus was on the top surface, net-to-gross, and fault model uncertainties and heterogeneities. While the authors emphasised on the importance of considering heterogeneity in the geothermal model, their approach of defining the optimisation function differs from this study. Blank *et al.* [2] showed that taking into account heterogeneous permeability structures may drastically affect the results in an optimal multi-well configuration around a major fault damage zone at the geothermal site Heiz-kraftwerk Süd in the Schäftlarnstraße (Munich). The permeability of the complex was based on values assigned for fault vs. elsewhere, and as such the heterogeneities considered in this work are distinctly different.

We note that there are various optimization studies carried out on high enthalpy deep Enhanced Geothermal Systems (EGS). However, due to significant technical differences between EGS and low enthalpy geothermal systems, we have not included them in this literature study.

1.2. Surrogate modelling for geothermal applications

The implementation of surrogate-based optimization and uncertainty quantification in the context of subsurface flow processes have been shown to be an effective tool to save computational expenses [12]. In the context of geothermal heat recovery, Vogt et al. [13] used kriging to address uncertainty in thermal conductivity of geothermal rocks. Due to computational cost of running multiple realizations, the stochastic modelling could produce a raw estimate of probability for temperature distribution. For this instance surrogate modelling could have served the purpose of reducing computational expenses of forward modelling. Chen et al. [14] used a multivariate adaptive regression spline technique to determine the optimal design of geothermal production operation in USA. Ansari et al. [15] used polynomial and kriging response surfaces, and they showed that the proxy models can be efficiently used to construct produced energy distribution from the geothermal parameters; distributions. Also for EGS, surrogates have been employed by Asai *et al.* [16] to determine optimal well placement. The authors found that this parameter is the most important one in the design of heat recovery from EGS. Pollack *et al.* [17] accounted for subsurface uncertainty by optimizing an EGS given an ensemble of reservoir models. The authors showed ignoring subsurface uncertainty and heterogeneity leads to over-optimistic NPV forecasts. Schulte *et al.* [1] used multi-objective particle swarm optimization to an ensemble of response surface models that were built using Gaussian process regression. A trade-off surface for the competing objective functions (maximizing heat production vs. minimizing the energy required for pumping) was obtained.

1.3. This study

Here we focus on optimization of *well/doublet spacing* for synthetic heterogeneous and fluvial geothermal systems with varying degrees of heterogeneity. We specifically focus on non-economic factors/outputs for which the operation of geothermal heat extraction should be optimized. For example, we purposely do not consider net present value (NPV), or the cost of drilling, and so on, for optimisation. Rather, we define the objective function solely based on the performance of the operation from fluid flow and heat transfer points of view. In doing so, we define an objective function that maximises heat recovery from a conventionally-defined licensed area around the doublet (a rectangle of size twice the well/doublet spacing), and maximises well performance through *Coefficient of Performance*. This is a novel approach for defining the objective function of the optimisation as it allows decoupling economic factors for heat recovery and allows to analyse effects of reservoir's heterogeneity on optimisation process separate from economic analyses. In comparison to [1], we have combined their multiple objective functions into one, but also added the emphasis of maximizing heat recovery from a target licensed area to ensure a sustainable heat extraction strategy by minimising interference to the surrounding license regions. The minimisation of interference is crucial in preserving the heat from neighbouring resources as discussed by [18].

In implementing the optimisation, we consider two algorithms (simple-search and advanced). For the first algorithm, we simply construct a surface based on the input variables (well and doublet spacings) over a structured mesh, and then by looking at the surface, the

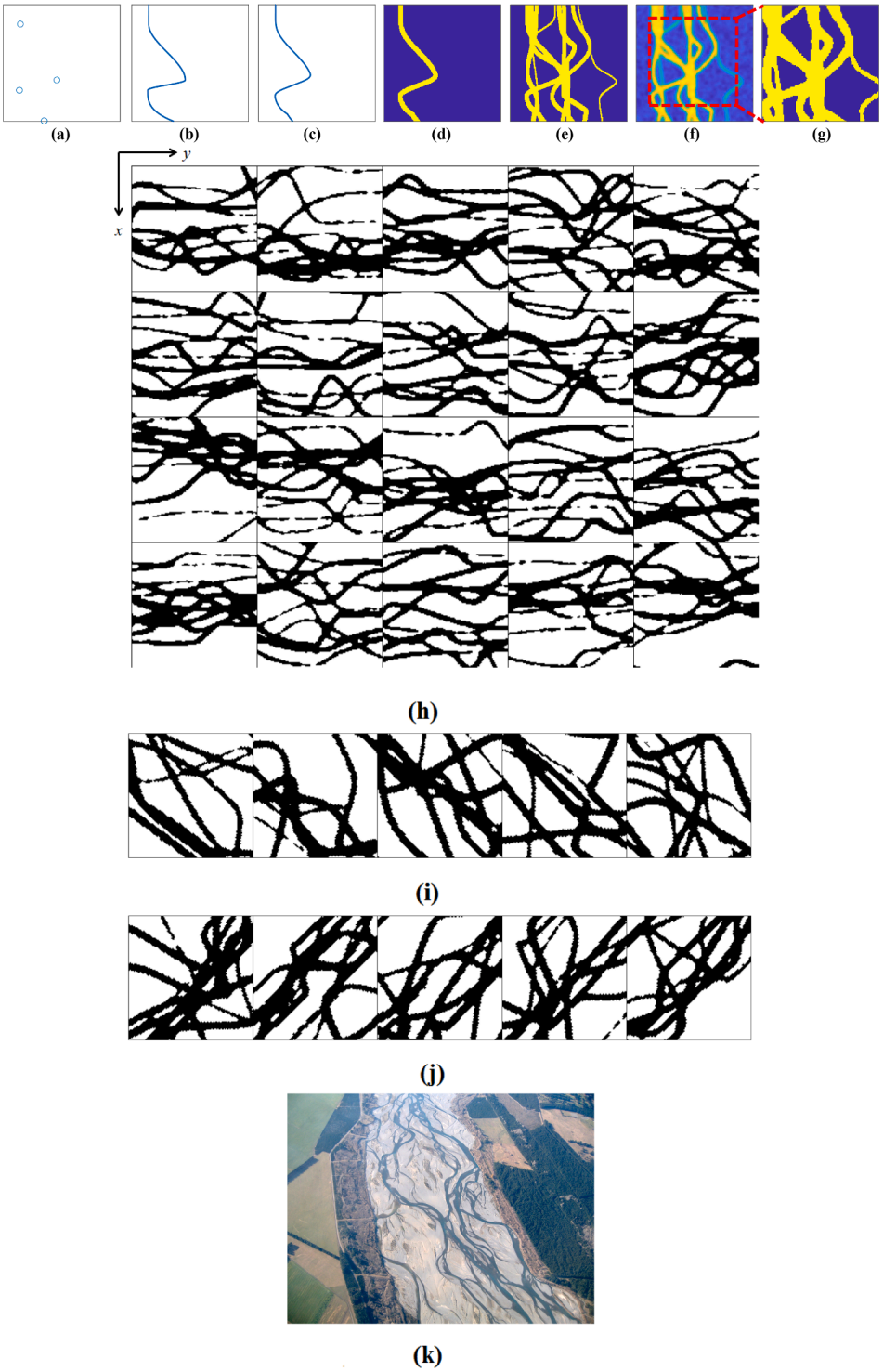

Fig. 2. (a to g) Process of constructing realisations of braided channels in *x*-direction based on the Piecewise Cubic Hermite Interpolating Polynomial method. (h) 20 realisations of braided channels in *y*-direction. Each panel is 120 by 120 in resolution. Black represents channels, (i) 5 first (out of 20) realisations of braided channels with 45° orientation, (j) 5 first realisations of braided channels with −45° orientation, and (k) Waimakariri river in New Zealand, an example of the braided pattern.

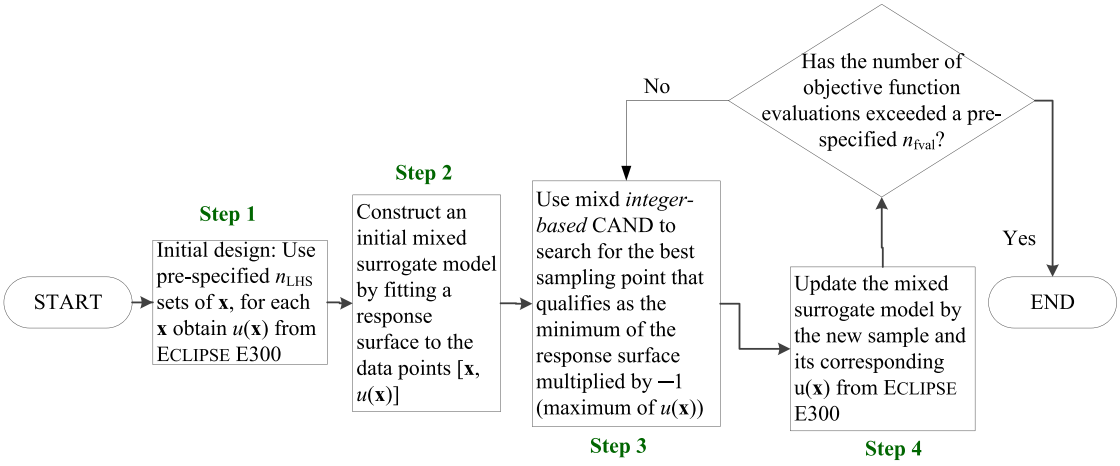

Fig. 3. The flowchart of the surrogate-based optimisation algorithm.

Table 2
Simulation cases defined for this study. We note that n_r for 3D is 8, and for 2D is 20.

Sim. case	Q [m^3/hr]	Case	Run format	Life-time [years]	Number of simulations
I	250	3D Homogeneous	Simple-search	LT = 15	10 × 10
II	250	3D Homogeneous	Simple-search	LT = 30	10 × 10
III	250	3D Homogeneous	Simple-search	15 <LTP1 <30	10 × 10
IV	250	3D Heterogeneous	Simple-search	LT = 15	4 het. cases × 10 × 10 × n_r
V	250	3D Heterogeneous	Simple-search	LT = 30	Het. cases 1 and 2 × 10 × 10 × n_r
VI	250	3D Heterogeneous	Optimisation	15 <LTP1 <30	4 het. cases × n_{fval} × n_r
VII	150	3D Homogeneous	Simple-search	LT = 15	10 × 10
VIII	150	3D Homogeneous	Simple-search	LT = 30	10 × 10
IX	400	3D Homogeneous	Simple-search	LT = 15	10 × 10
X	400	3D Homogeneous	Simple-search	LT = 30	10 × 10
XI	150	3D Heterogeneous	Optimisation	15 <LTP1 <30	4 het. cases × n_{fval} × n_r
XII	400	3D Heterogeneous	Optimisation	15 <LTP1 <30	4 het. cases × n_{fval} × n_r
XIII	250	2D braided in *y*-direction	Simple-search	LT = 15	10 × 10 × n_r
XIV	250	2D braided in *y*-direction	Simple-search	LT = 30	10 × 10 × n_r
XV	250	2D braided 45° orientation	Simple-search	LT = 15	10 × 10 × n_r
XVI	250	2D braided −45° orientation	Simple-search	LT = 15	10 × 10 × n_r

optimal location is identified. Of course, this method is computationally time-consuming. For the second approach, we use surrogate response surface modelling. This method is more computationally efficient than the basic algorithm.

Based on the above, the present study has the following novelty aspects:

- Definition of a geothermal objective function that is based on a licence area rather than a whole domain;
- Consideration of various forms of heterogeneity through multiple realisations (8 for correlated heterogeneity and 20 for fluvial settings);
- Employing surrogate surfaces for efficient optimisation and comparison with a simple search for extrema;

The paper is presented in the following sections. In Section 2, the synthetic heterogeneous geothermal model to be used is defined, and rock and fluid properties are presented. In Section 3, the surrogate modelling is briefly presented, optimisation state variables and objective functions are defined, the optimisation algorithm is presented and simulation runs are introduced. In Section 4, the results are presented. The conclusions and future works are presented in Section 5.

2. Geothermal models

2.1. Geometry, initial conditions, and meshing

We use two sets of models in this work. The first one is a 3D model of homogeneous and heterogeneous (with spatial correlation) of low-enthalpy aquifers, as described in the following.

2.1.1. Spatially correlated model (3D)

The domain is a 3D rectangle with the size of 3 km × 3 km × 500 m in *x*, *y*, and *z* directions, with an overburden of 200 m thickness, an aquifer of 100 m thickness, and an underburden of 200 m thickness. We use uniform 120 × 120 mesh laterally. For vertical direction, the overburden and underburden are represented each with one layer only. The aquifer has 10 layers. Overall, there are 12 layers and 172,800 gridblocks in the model. The top of the model is 2,250 m deep. p_{init} is 200 bar (initial pressure), and T_{init} is 67.5 °C (initial temperature) at top of the reservoir with 3 °C/100 m temperature gradient. The boundaries are close to flow around all the sides. For an illustration of model geometry, we refer to our previous publication [19] (Fig. 1).

The rock's properties are set as: thermal conductivity 0.91 W/m/K, density 2650 kg/m^3, specific heat capacity 2,000 J/kg/K, and

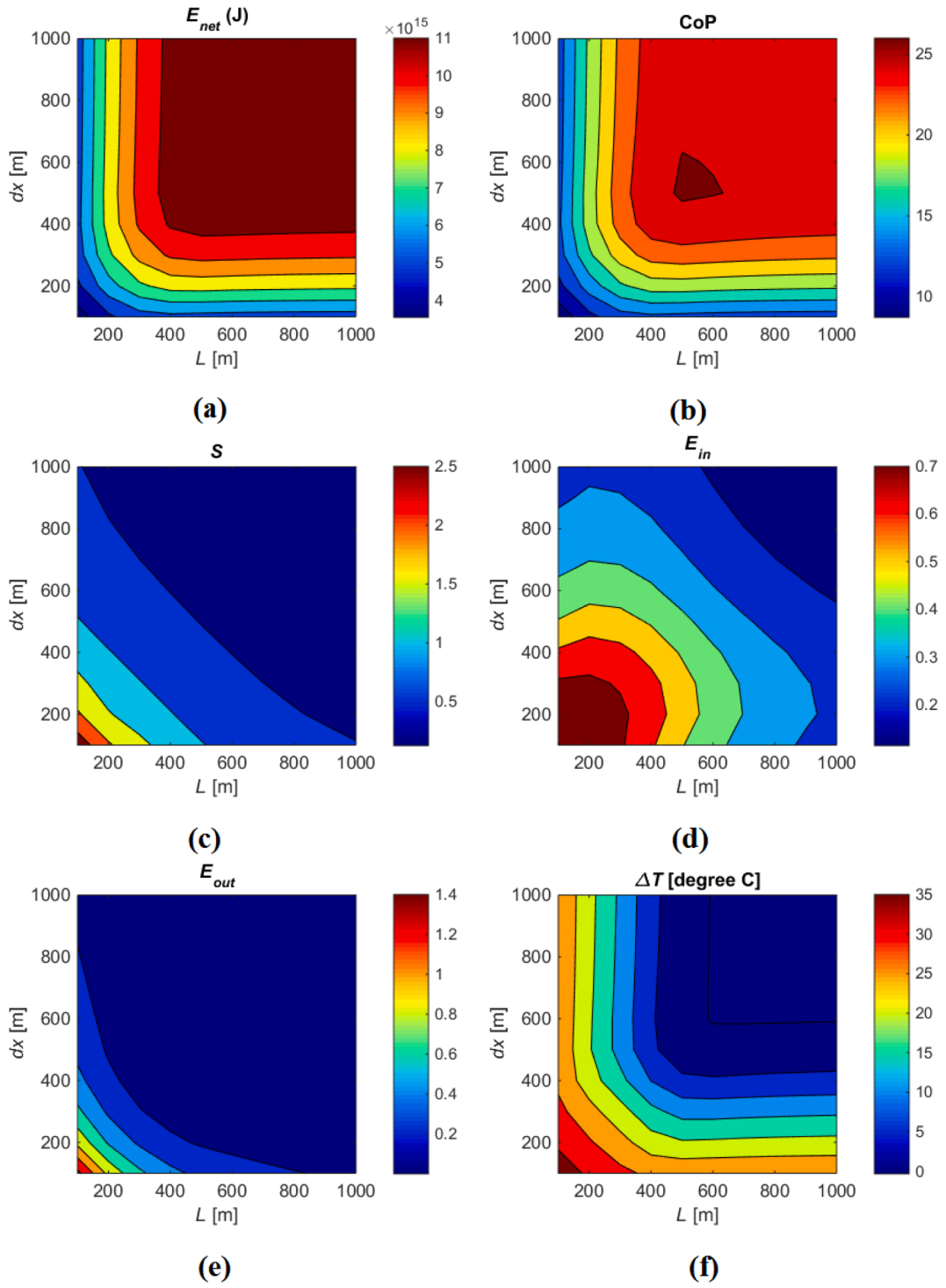

Fig. 4. The outputs for simulation case I, (a) E_{net}, (b) CoP, (c) S, (d) E_{in}, (e) E_{out}, and (f) production ΔT at fixed life time of 15 years.

compressibility 4.93×10^{-5} bar^{-1} at 250 bar. Overburden/underburden porosity and permeability are 0.01 and 0.001 mD, respectively. An available code [20] is used to generate spatially correlated porosity fields with different lateral correlation lengths. The method utilizes the Fourier-transform of the covariance function as the power spectral density function of all realizations. Random autocorrelated fields are generated by creating random phase spectra meeting the conditions of real numbers in the physical domain. The realizations are then converted by back-transformation of the power- and phase-spectrum into the physical domain [20].

The porosity fields have a mean of 0.17, and a variance of $\sigma^2 = 0.04$. The correlation lengths in lateral directions (here c_x denotes the x-direction correlation length and c_y denotes the y-direction correlation length) are: (1) $c_x = 100$ m, $c_y = 100$ m; (2) $c_x = 1000$ m, $c_y = 200$ m; (3) $c_x = 100$ m, $c_y = 1000$ m rotated 45 ° anticlockwise; and (4) $c_x = 100$ m, $c_y = 1000$ m rotated 45 ° clockwise. Here by $c_x = 100$ m, we mean the correlation length in x direction is 100 m which corresponds to 4 grid-blocks in our model. In other words for $cx = cy = 100$ m, we expect correlated permeability circles with radius of 100 m throughout the domain. Eight realisations are generated for each case. The following

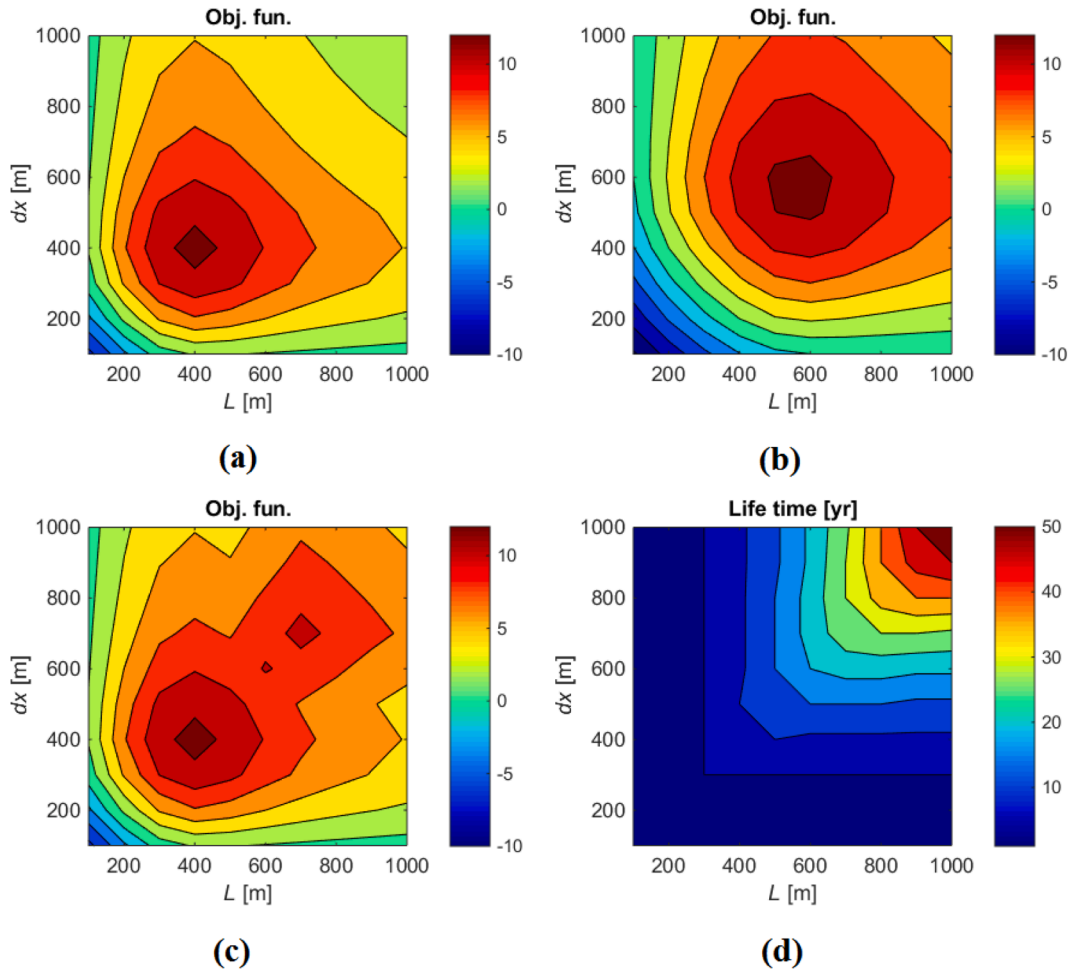

Fig. 5. (a) The objective function distribution for simulation case I, (b) the objective function distribution for simulation case II, (c) the objective function distribution for simulation case III, and (d) LTP1 (life time when there is 1 °C drop at wells obtained for a simulation without fixing or restricting the life times).

relationship based on Delft Sandstone aquifers in the Netherlands [21] is used to derive permeability from porosities:

$$K = -2.03 \times 10^{-7}\phi^5 + 2.55 \times 10^{-5}\phi^4 - 1.04 \times 10^{-3}\phi^3 + 8.91 \times 10^{-3}\phi^2 + 3.58 \times 10^{-1}\phi - 3.21 \times \phi^0 \quad (1)$$

Similar realizations are depicted in Babaei and Nick [19] (Fig. 3). In addition to the heterogeneous 3D cases above, we define a 2D homogeneous case for comparison. For this case ϕ= 15%, and K = 139 mD (based on Eq. 1) everywhere in the domain. The statistics of all realisations are presented in Table 1.

2.1.2. Fluvial models (2D)

In order to test a more challenging system in terms of porosity and permeability distribution, channelised fluvial systems are considered in 2D. Specifically, braided channels are generated in the y-direction, 45° and −45° orientations. Braided channels exhibit numerous channels that split off and rejoin each other to give a braided appearance [22]. In order to make realistic representations of channels, we start by placing few random points in an elongated subsection of the image domain (Figs. 2,3a). Then using a fitting technique named Piecewise Cubic Hermite Interpolating Polynomial (PCHIP) [23], points are replaced with a curve (Fig. 2b). By applying moving average on the fitted curve, pointy corners will become smoother to imitate the shape of a natural channel (Fig. 2c). Afterward, we voxelized the line point and apply image dilation transform to add thickness to the created channel image (Fig. 2d). By repeating this process more channels are added to the image (Fig. 2e). It is also possible to select a random size for the dilation structural element and create channels with different thicknesses. Then, in order to add some irregularities to the image, we add it to an array of smoothed white noise (Fig. 2f) and perform thresholding and cropping the margins to reach the final binary map of the channel texture (Fig. 2g).

The maps of braided channels for 20 realisations in the x-direction are shown in Fig. 2(h). The domain is 3 km × 3 km × 100 m (no overburden or underburden). The size of the mesh is 120 × 120 × 1. The porosity is designated as 0.05 for non-channel areas, vs. 0.5 for channelled areas. The permeability is designated as 10 mD for non-channels areas vs. 4000 mD for channelled areas. All other properties (thermal conductivity of rock, rock density, rock specific heat capacity, and rock compressibility) are the same as the 3D model. The top surface of the aquifer is 2450 m deep, the initial pressure is 200 bar, and the initial temperature is 75 °C.

2.2. Other modelling remarks

Two doublets with a checkerboard pattern similar to [18] are used for heat extraction. The injection wells (I1 and I2), and the production wells (P1 and P2) are positioned so that the distance between each doublet is L, and the distance between the two doublets is dx. I1 is positioned always at x = 750 m and y = 750 m. Whereas, I2, P1, and P2 will be positioned according to L and dx. The temperature of the injected water is 30 °C. The maximum permissible (upper limit) bottomhole pressure of the injection wells is set to 260 bar. In case of nearing this value, the injection rate is decreased automatically. Cold water is

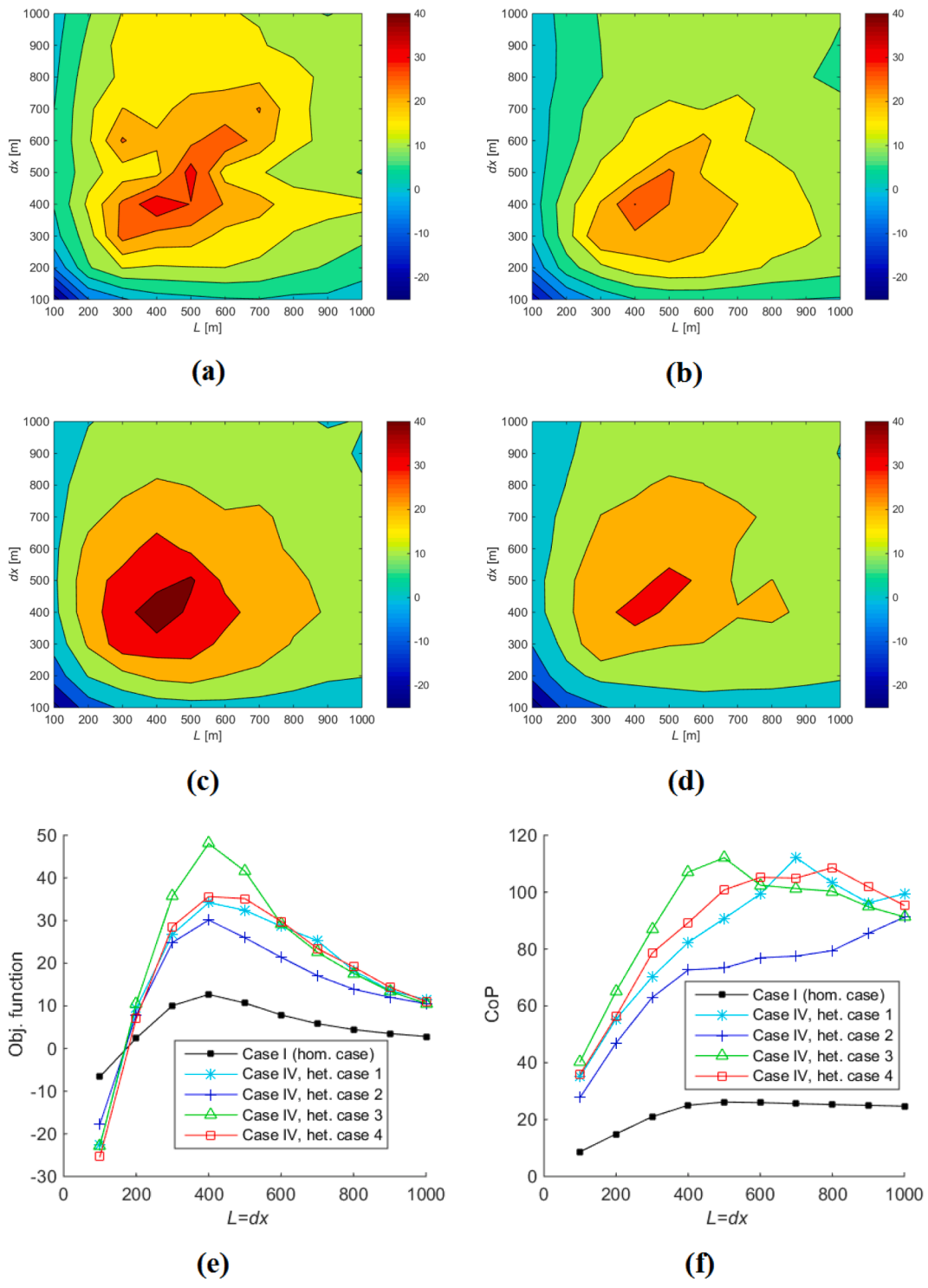

Fig. 6. The objective function distribution for simulation case IV for (a) heterogeneous realisations of case 1, (b) heterogeneous realisations of case 2, (c) heterogeneous realisations of case 3, (d) heterogeneous realisations of case 4, (e) objective function values vs. $L = dx$, and (f) CoP values vs. $L = dx$.

Table 3
Optimisation results for simulation case IV.

Simulation case	Heterogeneity case	Optimal L [m]	Optimal dx [m]	Optimal obj. function value
IV	1	400	400	34
IV	2	400	400	30
IV	3	400	400	48
IV	4	400	400	36

injected using the well injection rate of Q. For 3D, the wells are perforated only into the aquifer (10 layers), and for 2D there is obviously only one perforation.

Local thermal equilibrium was assumed for each gridblock, meaning that heat efficiently and instantly is conducted from solid to fluid, making the Biot number much smaller than 1. As such, we can assume the temperature of the solid and fluid phases in each gridblock is identical [24]. All simulations of this study are carried out by ECLIPSE E300 simulator [25]. The governing equations are described in detail in

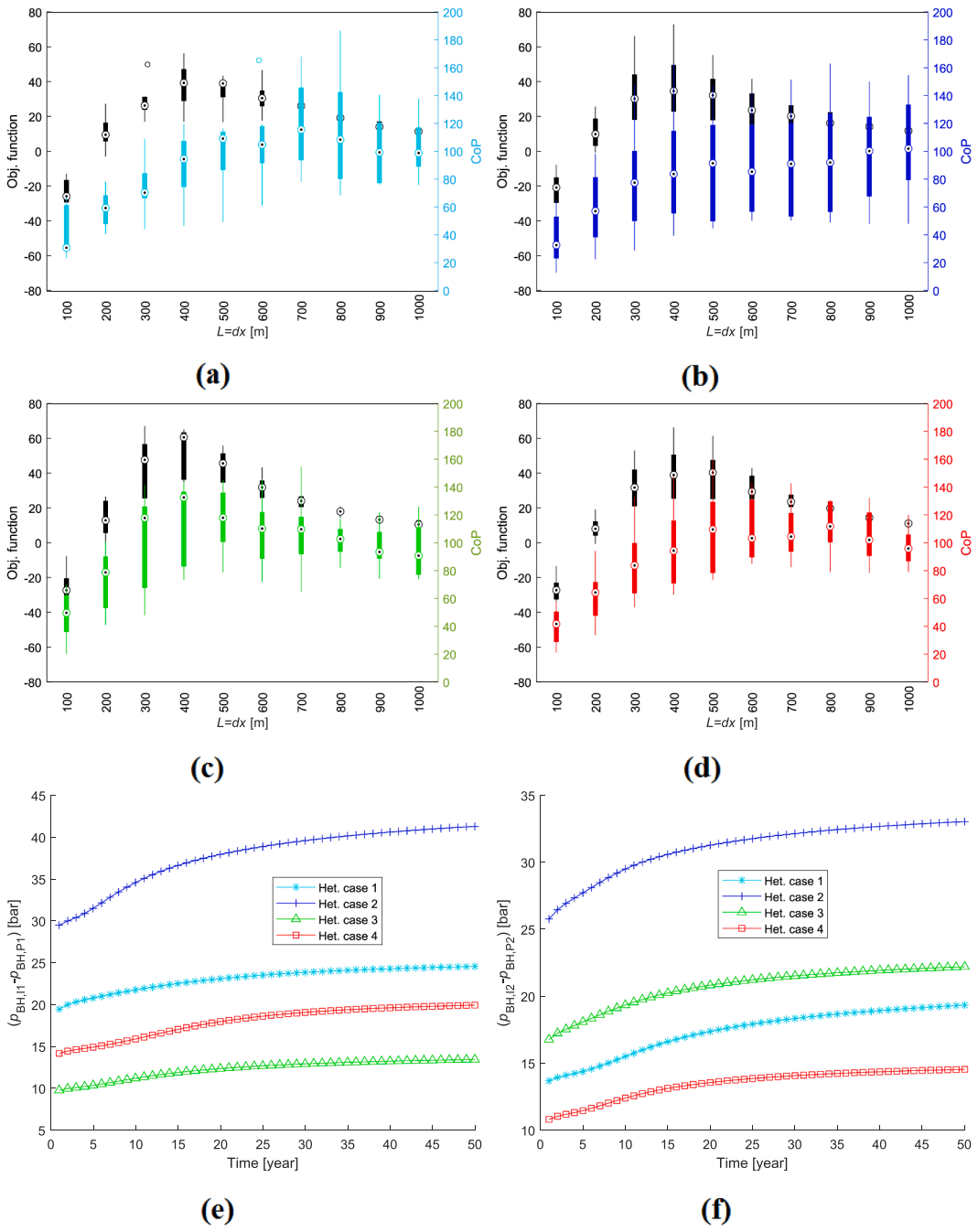

Fig. 7. Box plots of simulation results vs. $L = dx$from case IV with 8 realisations (objective function and CoP separately calculated for each realisation). (a) Heterogeneous realisations of case 1, (b) heterogeneous realisations of case 2, (c) heterogeneous realisations of case 3, (d) heterogeneous realisations of case 4. (e) $< \Delta p_{BH1} >$ vs. time for $L = dx = 400$ m, and (f) $< \Delta p_{BH2} >$ vs. time for $L = dx = 400$ m.

[25,19].

3. Methodology

3.1. Optimisation state variables and objective function

The optimisation problem is defined based on a set of state variable or variables ($\mathbf{x}$) and objective or objectives ($\mathbf{u}$), so that $\mathbf{u}(\mathbf{x})$ is optimised. The state variables in this study are the well/doublet spacing (L, dx) as shown in Fig. 1. The minimum and maximum spacing are set to be 100 m and 1300 m, respectively. That is, while the position of the well I1 is fixed (750 m in x and y directions from the top left corner of the domain), P1 and P2 can be positioned anywhere between 850 m and 2050 m from the top left corner. The position of I2 is correspondingly changed with respect to the positions of P1 and P2.

A single objective function is defined based on the well and reservoir behaviour (*i.e.*, no economic model is integrated into the optimisation). The optimisation function should be defined in such a way that it includes and accounts for the performance measures of the geothermal system. To define the objective function based on these objectives, several definitions are required as follows.

Licensed region's boundary: this is the shell-like lateral inner boundary blocks of the license area. The license area is taken as the $2L \times 2dx \times$ 10-layer rectangle around the wells as shown in Fig. 1.

Average temperature of production wells

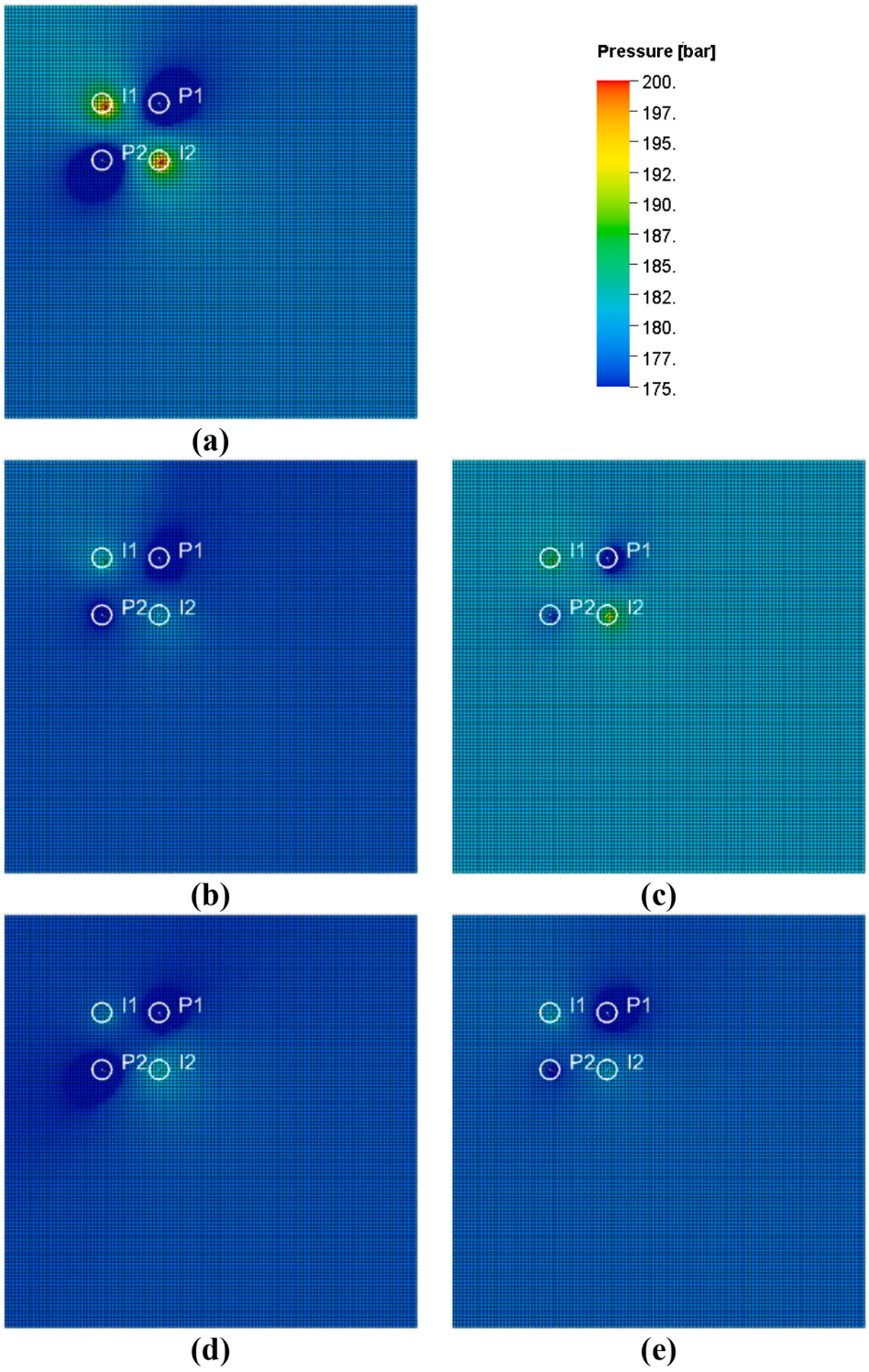

Fig. 8. The pressure distribution at the end of the operation (year 50) across the top layer of (a) the homogeneous case, (b) the heterogeneous case 1, (c) the heterogeneous case 2, (d) the heterogeneous case 3, and (e) the heterogeneous case 4.

$$< T^t_W >= \frac{\int_{k=1}^{10} q^{prd,t}_{W,k} T^t_{ijk}}{\int_{k=1}^{10} q^{prd,t}_{W,k}} \tag{2}$$

where $q^{prd,t}_{W,k}$ is the production rate of water at layer k for well W, at time t. T^t_{ijk} is the temperature of gridblock ijk at time t. The denominator is constant $Q_{prd,W} = \int_{k=1}^{10} q^{prd,t}_{W,k}$.

Life time based on (average) production: LTP1 is defined as the time (in years) when $< T^t_P >= \frac{<TW^t_{P1}>+<TW^t_{P2}>}{2}$ drops 1 °C compared to the initial condition. As it can be the case that for small *L*and *dx*values, the value of life time becomes too small (from operational point of view) and conversely for large *L*and *dx*values, the value of life time becomes too large, we have set the constraint that 15 years <LTP1 <30 years.

Life time fixed: Life time is a fixed 15-year or 30-year of operation regardless of the temperature drop in the wells. We can determine the production temperature drop at any LTP including the fixed 15-year or

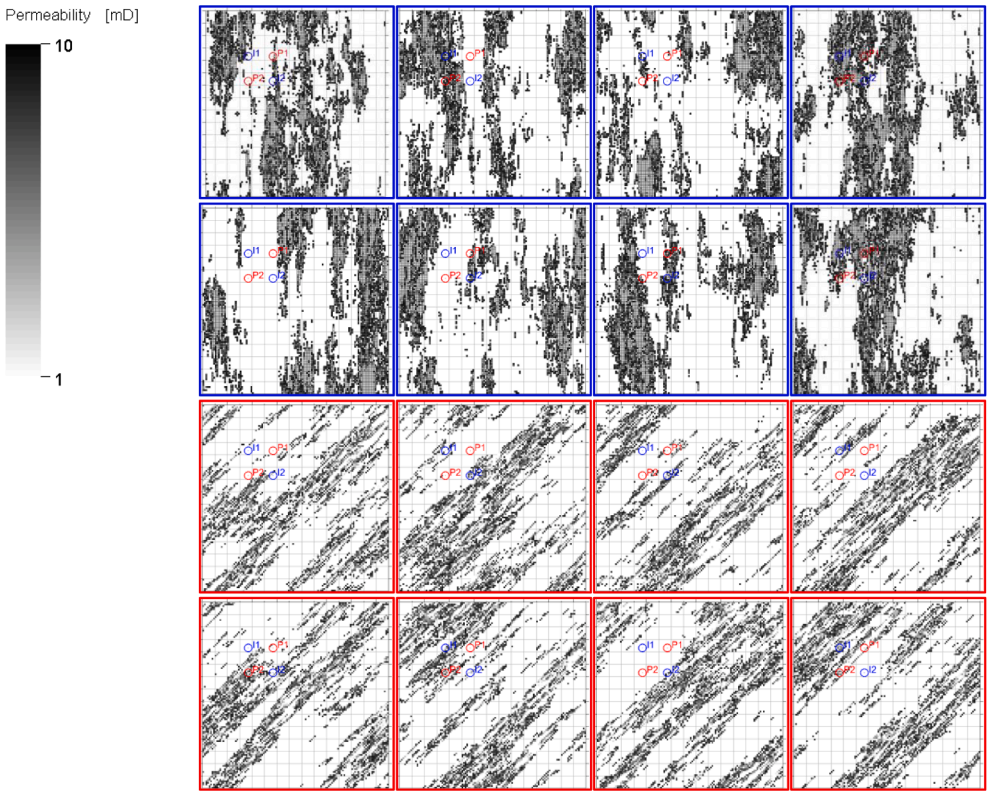

Fig. 9. The low permeability distribution in the domain (K< 10 mD) for realisations of the heterogeneous case 2 (the first 8 subfigures), and the heterogeneous case 3 (the second 8 subfigures).

30-year life time.

Coefficient of Performance is a dimensionless property defined as:

$$\mathrm{CoP} = \frac{E_{\mathrm{prod}}}{E_{\mathrm{pump}}}, \tag{3a}$$

$$E_{\mathrm{prod}} = (\rho C)_w Q \int_{t=0}^{\mathrm{LTP}} \left(\langle T'_W > -T_{inj}\right) dt, \tag{3b}$$

$$E_{\mathrm{pump}} = \frac{Q}{\varepsilon} \int_{t=0}^{\mathrm{LTP}} \left(\langle p_{\mathrm{inj}} - p_{\mathrm{prd}} > \right) dt \tag{3c}$$

where E_{prod} is the produced energy and E_{pump} is the pump energy losses based on [26]. ε is the pump efficiency (%60), and $< p_{\mathrm{inj}} - p_{\mathrm{prd}} >$ is an averaged pressure difference of two doublets:

$$\langle p_{\mathrm{inj}} - p_{\mathrm{prd}} \rangle = \frac{\langle p_{\mathrm{BH,I1}} - p_{\mathrm{BH,P1}} \rangle + \langle p_{\mathrm{BH,I2}} - p_{\mathrm{BH,P2}} \rangle}{2}, \tag{4}$$

where $p_{\mathrm{BH,W}}$ refers to the bottomhole pressure of well W, so that $\langle p_{\mathrm{BH,I1}} - p_{\mathrm{BH,P1}} \rangle$ is the averaged over all realisations of bottom-hole pressure differences between well I1 and P1.

Net Energy defined as:

$$E_{\mathrm{net}} = E_{\mathrm{prod}} - E_{\mathrm{pump}}, \tag{5}$$

Energy Sweep indicates how efficiently heat is extracted. This is defined as:

$$S = \frac{E_{\mathrm{prod}}}{E_R}, \tag{6a}$$

$$E_R = \int_{i=1}^{N_b} (\rho_w C_w \phi_i + \rho_r C_r (1-\phi_i)) \left(T_{\mathrm{init},i} - T_{\mathrm{inj}}\right) dV_{bi}. \tag{6b}$$

where E_R is the reservoir energy of the license area ($2L \times 2dx \times 10$layers surrounding the doublets), V_{bi} is the volume of gridblock i in the license area, N_b is the number of gridblocks in the license area, and E_{prod} is the geothermal energy recovered by the doublets during the lifetime of the operation.

The optimisation algorithm attempts to maximise the following dimensionless objective function with state variables L and dx, and for various rates of injection at a life time (either LTP1 or fixed LTP) as:

$$f = (E_{\mathrm{in}} - E_{\mathrm{out}}) \times \mathrm{CoP}, \tag{7}$$

where $E_{\mathrm{in}}$is the average (over all the realisations) of the thermal depletion *inside* the licence area of the reservoir at the lifetime divided by E_R:

$$E_{\mathrm{in}} = \frac{\int_{i=1}^{N_b} (\rho_w C_w \phi_i + \rho_r C_r (1-\phi_i)) \left(T_{\mathrm{init},i} - T_{\mathrm{LTP,i}}\right) dV_{bi}}{E_R}, \tag{8}$$

whereas $E_{\mathrm{out}}$is the average (over all the realisations) of the thermal depletion *outside* the licence area of the reservoir at the lifetime divided by E_R:

$$E_{\mathrm{out}} = \frac{\int_{i=1}^{N_{\mathrm{out}}} (\rho_w C_w \phi_i + \rho_r C_r (1-\phi_i)) \left(T_{\mathrm{init},i} - T_{\mathrm{LTP,i}}\right) dV_{bi}}{E_R}. \tag{9}$$

where N_{out} is the number of gridblocks outside of the licence region.

Defining the objective function based on Eq. 7 dictates that E_{in} must be maximised while E_{out} must be minimised, at the same time CoP (which is based on the well performance) should also be maximised. With this definition, no economic constraint or variable is needed for optimisation and the solution is optimised merely based on the performance over the domain and wells in the geothermal aquifer system. Also as it is dimensionless, the performance of different systems can be compared with each other.

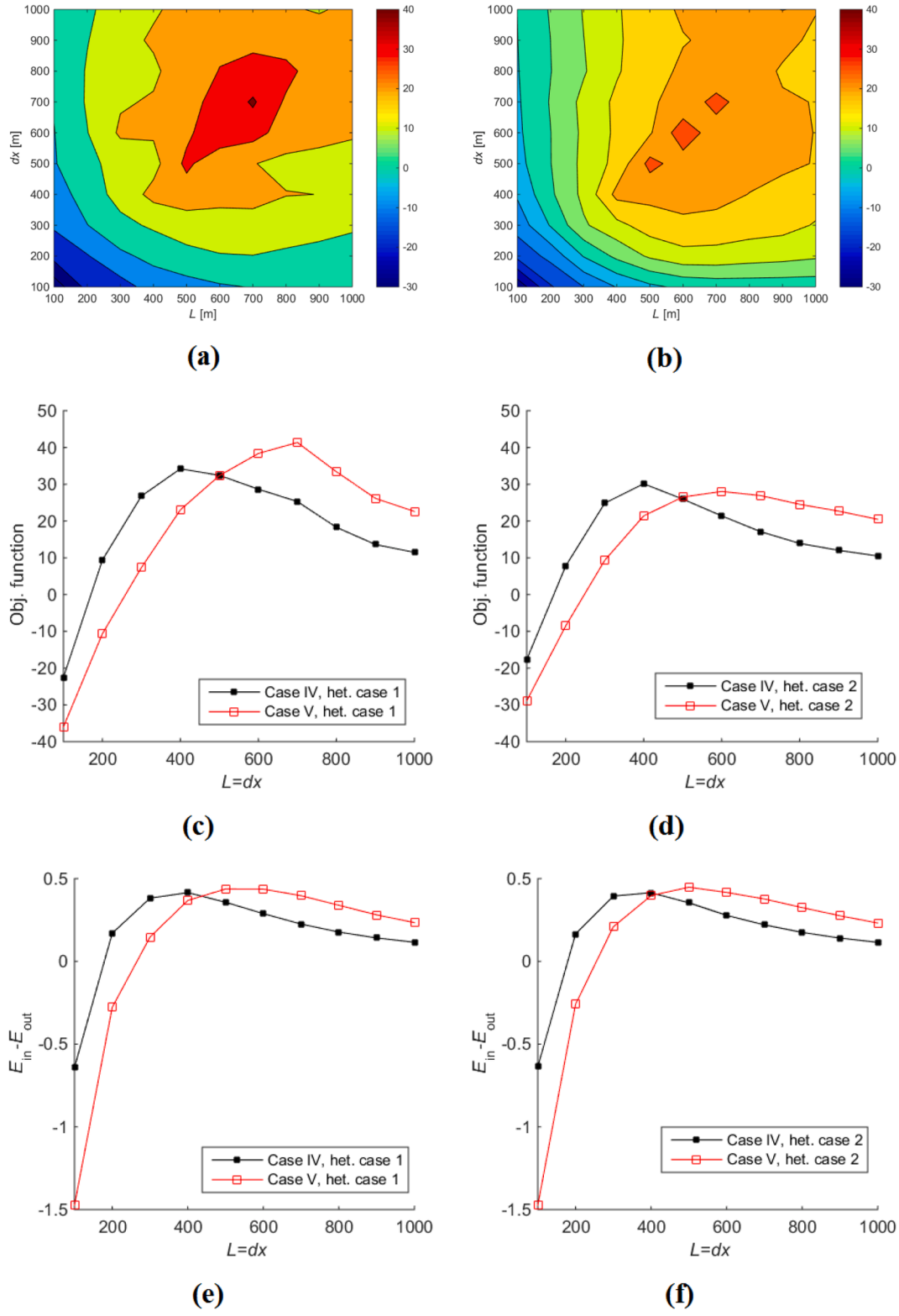

Fig. 10. The objective function distributions for simulation case V for (a) heterogeneous realisations of case 1, and (b) heterogeneous realisations of case 2. Comparing results of simulation case IV (life time fixed 15 years) and V (life time fixed 30 years) for (c) objective function of heterogeneous case 1, (d) objective function of heterogeneous case 2, (e) $E_{in} - E_{out}$ of heterogeneous case 1, and (f) $E_{in} - E_{out}$ of heterogeneous case 2.

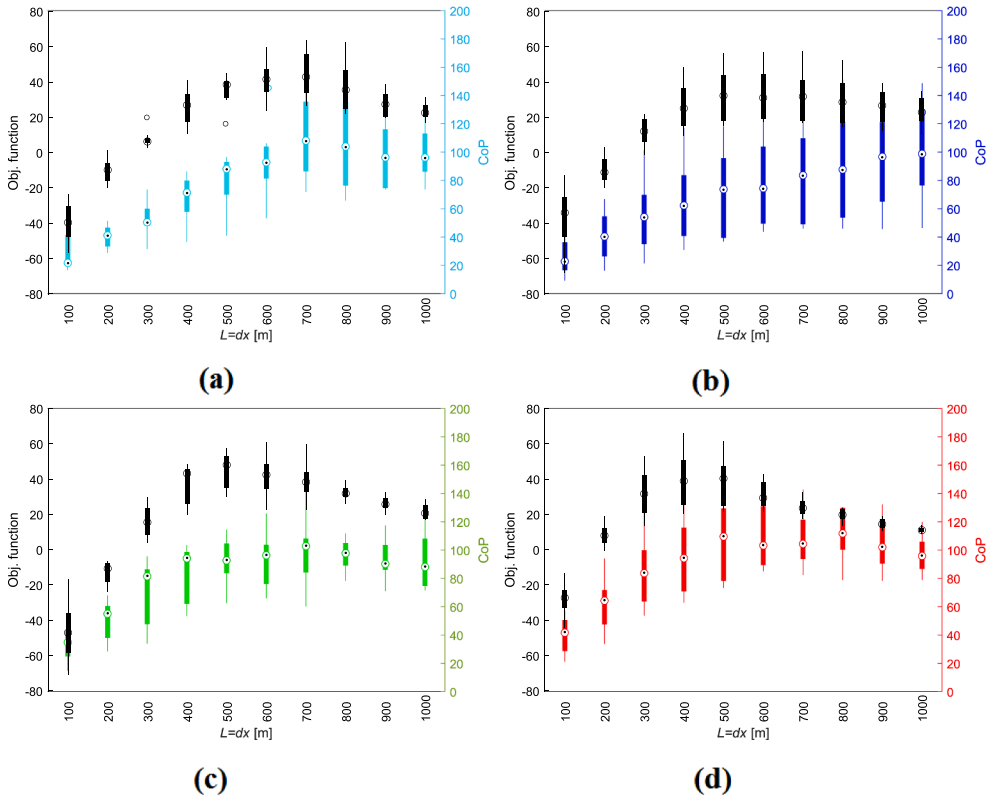

Fig. 11. Box plots of simulation results vs. $L = dx$ from case V with 8 realisations (objective function and CoP separately calculated for each realisation). (a) Heterogeneous realisations of case 1, (b) heterogeneous realisations of case 2, (c) heterogeneous realisations of case 3, and (d) heterogeneous realisations of case 4.

3.2. Surrogate modelling

In this work, surrogate modelling is carried out by the Modularized Surrogate Model toolbox [27], developed in MATLAB. Between various surrogate models, we use cubic Radial Basis Functions (RBF), as Babaei and Pan [28] showed that RBF is consistently the best and computationally the most efficient surrogate model. This conclusion has been made for complex hydrocarbon recovery optimization using surrogate modelling comparing the performance of cubic RBF with Gaussian kriging and Multivariate Adaptive Regression Splines. The results demonstrated that the radial basis function is reliable consistently for optimization problems in subsurface engineering.

3.3. Optimisation algorithm using surrogate modelling

By writing the objective function as $u(x)$, where $u$can be the objective function of Eq. 7, and x can be Lor dx, the surrogate-based optimisation algorithm of [29] (Fig. 6) is employed. Here we have, $u(x) = \frac{\sum_{i=1}^{n} u_i(x)}{n_r}$, where $i$is realisation number from 1 to n_r, where $n$is the number of realisations that in this study $n_r = 8$.

The components of the optimisation algorithm include sampling by Latin Hypercube Sampling (LHS) scheme (Step 1), construction of the initial surrogate model (Step 2), using CAND (Candidate Point Strategy) to find the minimum value of $-u(x)$ (maximum of $u(x)$) (Step 3), and updating the surrogate model based on new candidate point function evaluations (Step 4). These are shown in the flowchart of Fig. 3.

The algorithm generates an experimental design using LHS. We need at least $n_{\mathrm{LHS}} = n_x + 1$ initial design sites for building the surrogate model [30], where n_x is the number of state variables. The number of sampling points by Latin hypercube sampling is denoted by n_{LHS}. The maximum allowable number of function evaluations, n_{fval}, is specified by the user. Using Candidate Point Strategy [31], the sampling points are perturbed and different groups of candidate sampling points are obtained. The perturbation mechanism generates integer feasible sampling points for well/doublet spacing and continuous feasible sampling points for injection rate.

3.4. Simulation runs

Overall we define the simulation runs summarised in Table 2 using 2D and 3D models defined in Section 2.1. In this table, by *simple-search* for running the simulations we mean simulations are carried out in a mesh of 10 by 10 locations for L and dx, where 100 m $< L <$ 1000 m, and 100 m $< dx <$ 1000 m. For the optimisation runs we assign $n_{\mathrm{LHS}} = 8$, and $n_{\mathrm{fval}} = 20$. The simple-search format will incur more computations. Nevertheless, the advantage is that the surfaces for the objective function and other outputs of simulations can be constructed over an even mesh.

4. Results

4.1. Cases I, II, and III (3D Homogeneous cases, effects of life time variation)

In Fig. 4 we have shown all the outputs of simulation case I. The figure shows that with increase in $L$and dx until $L = dx = 600$ m, E_{net} [J] and CoP increase (the latter through increase in E_{prod}). This is expected as a larger area is available for production in a fixed 15-year production life time. E_{net} plateaus for larger values of $L$and dxas within a fixed life time of 15 years, it is not possible to produce more energy. In contrast, by increase in L and dx, S, E_{in} and E_{out} decrease steeply. S decreases because $E_R$increases much more than E_{prod}increases for a larger domain of heat extraction. Similarly, based on Eqs. 8 and 9, the numerators increase less than the denominator (E_R) does, so that the ratios of heat extraction from inside and outside of the license area decrease over larger domains. Combining $E_{\mathrm{in}}, E_{\mathrm{out}}$ and CoP (all dimensionless) results

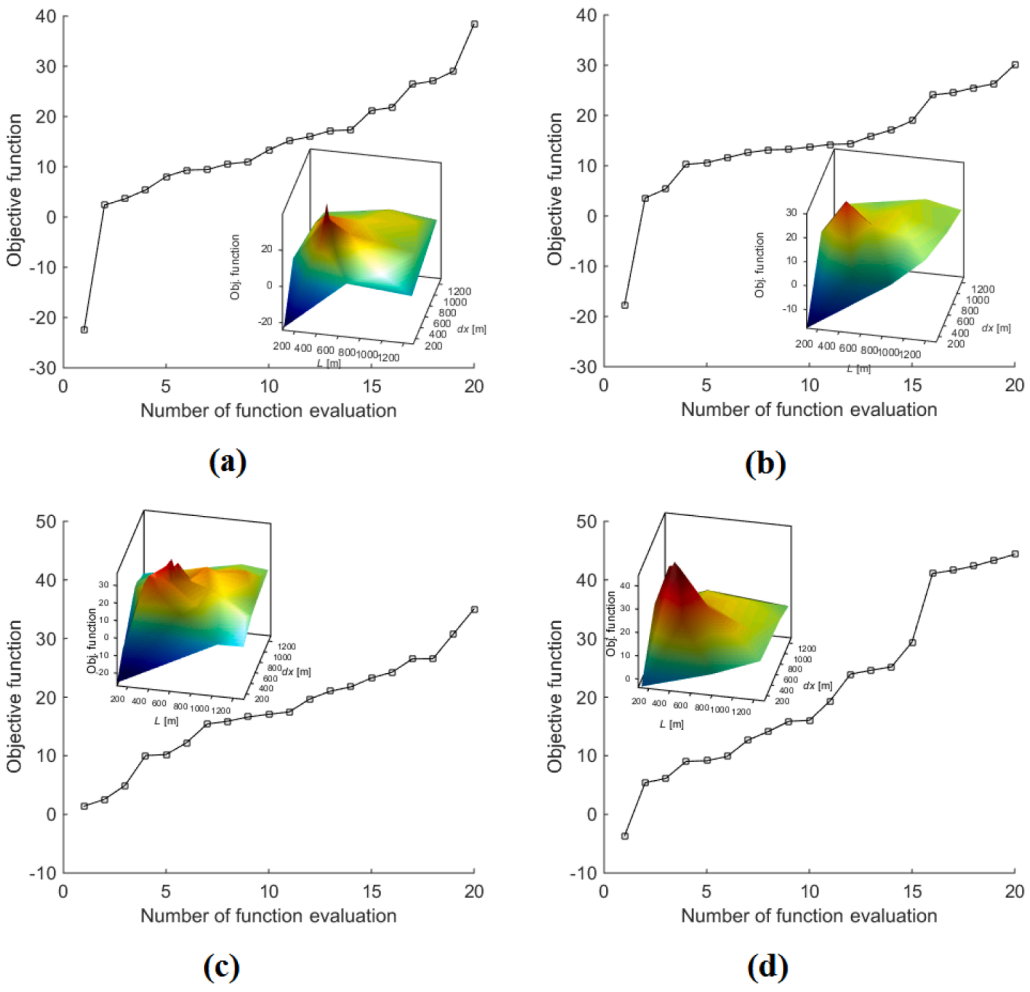

Fig. 12. Main plots: the objective function for each function evaluation ($n_{\text{feval}} = 20$) in optimisations of simulation case VI, for (a) heterogeneous case 1, (b) heterogeneous case 2, (c) heterogeneous case 3, and (d) heterogeneous case 4. Insets: the surfaces for objective function generated using all the function evaluations of optimisation.

Table 4
Optimisation results for simulation case VI.

Simulation case	Heterogeneity case	Optimal L [m]	Optimal dx [m]	Optimal obj. function value
VI	1	425	425	38
VI	2	400	400	30
VI	3	375	400	43
VI	4	475	475	35

in the objective function that is maximised at $L = dx = 400$ m as shown in Fig. 5,6(a). Fig. 4(f) shows the temperature drop at production wells at the fixed life time of 15 years. As expected, we observe a significant temperature drop for short well/doublet spacing that operationally renders the thermal extraction process unappealing.

Fig. 5 shows the objective function distributions for the simulation cases I, II, and III. We have used interpolation between data points (shown with triangles in the surfaces) to make full surfaces over the range of *L*and *dx*values used in the simulations. For simulation cases II, the optimal solution is occurring at $L = dx = 600$ m. The only difference in the two surfaces obtained between simulation cases I and III as shown in Fig. 5, is for high *L*and *dx*. This is because as shown in Fig. 5(c) only for this region the life time obtained for simulation case III (LTP1) is not 15 years. The figure also shows that there is a steep shift between LTP1 of 15 years (set as the minimum) and LTP1 of 30 years (set as the maximum). Without the constraint of 15 years ⩽LTP1 ⩽30 years, the life time would look similar to Fig. 5(d) where the life time smoothly changes between 1 and 50 years. However, geothermal heat pump systems have an average 20+ year life expectancy for the heat pump itself [32]. Therefore we have set a minimum of 15 years for the life time, assuming that the temperature drops of further than 1 °C is acceptable by the operator.

4.2. Cases IV and V (Effects of correlated heterogeneity)

Fig. 6(a to d) show the surfaces obtained for the objective function by conducting simulation cases IV. The optimal solution is occurring consistently at $L = dx = 400$ m as reported in Table 3 regardless of heterogeneity. Also, the injectivity of the model is sustainable throughout simulations, meaning that the flow rate can be achieved in the injection wells without nearing the maximum permissible bottom-hole pressure of 260 bar. This is the observation for all other simulation cases using the 3D model.

Fig. 6(e) and (f) show, respectively, the objective function and CoP values obtained from simulations with respect to $L = dx$ values (that is the diagonals of the surfaces in Fig. 6(a to d)). Also for comparison the objective function and CoP values of the homogeneous case from simulation case I are added to Fig. 6(e and f). The objective function values for heterogeneous cases are higher than the homogeneous case. This is because the CoP for heterogeneous cases is higher than the homogeneous case. The homogeneous case has a lower average value for

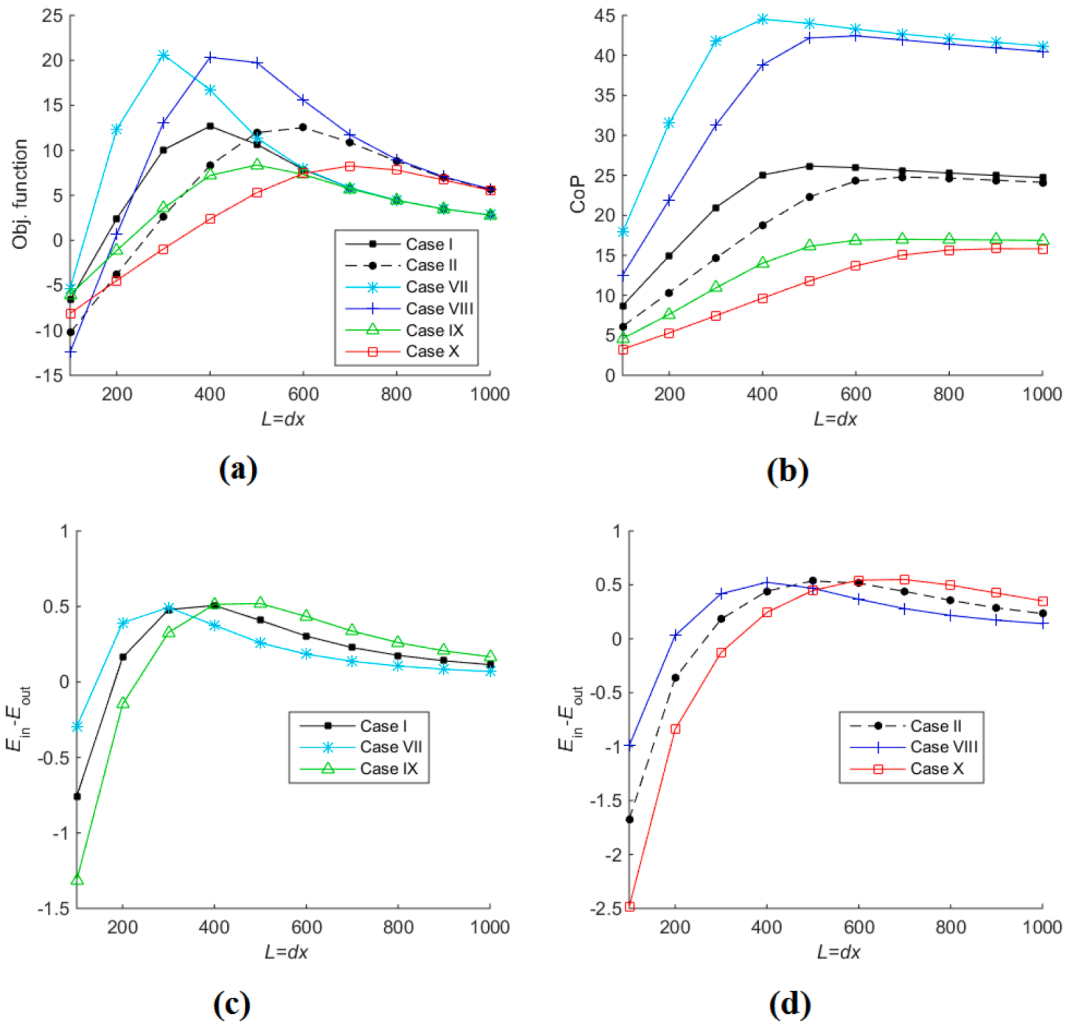

Fig. 13. Comparison between the results of simulation cases VII to X with simulation cases I and II, (a) objective function values with respect to diagonal values of the simple-search format for L and dx, (b) CoP, (c) $E_{in} - E_{out}$ for cases I, VII and IX, and (d) $E_{in} - E_{out}$ for cases II, VIII and X.

permeability than the heterogeneous cases, therefore, the pressure differences are higher for the homogeneous case compared with the heterogeneous case.

The definition of the objective function has masked the differences between heterogeneous cases. While CoP values and optimal locations for highest CoPs are different between the heterogeneous cases, the multiplication of $E_{in} - E_{out}$ into CoP makes the optimal location consistently happening at 400 m. This is shown further in Fig. 7, where we have run the case IV simulations for each individual realisations of four heterogeneous cases separately. It is clear that CoP has different optimal values for L and $dx$for different heterogeneity cases. For example by examining the median of box plots for CoP in Fig. 7 (coloured boxes), heterogeneity case 1 has an optimal value of 700 m for CoP, heterogeneity case 2 shows a steady increase in CoP as the distances increase, heterogeneity case 3 has an optimal value of 400 m for CoP, and heterogeneity case 4 has an optimal value of 800 m for CoP. Also, we observe larger variations in CoP values at each L or dx for heterogeneity case 2 compared with other cases. This shows large pressure difference variations between different realisations at a fixed life time of 15 years for heterogeneity case 2. As also shown in Fig. 6, the black boxes for the objective function show a consistent 400 m optimal location for all different heterogeneity cases. Therefore it is clear that the definition of objective function has put emphasis on optimising heat recovery from within the license area and as such, the differences between different heterogeneity cases with respect to the optimal well/doublet spacing have been minimised.

The reason why the heterogeneity case 2 shows increasing CoP with increasing L and dx, is that for this case pressure difference between wells remains high throughout the simulations, therefore, the higher distances alleviate the pressure difference leading to improved CoPs. This is not the case for other heterogeneity cases. We have chosen $L = dx = 400$ m as an example to report the average well pressure differences over time as shown in Fig. 7(e and f) for $\langle p_{BH,I1} - p_{BH,P1} \rangle$ and $\langle p_{BH,I2} - p_{BH,P2} \rangle$. Also in this figure, we can see higher average well pressure differences for heterogeneous case 2 compared with other heterogeneous cases. Shown visually in Fig. 8, we plotted the pressures retained in the system after 50 years of operation. Heterogeneous case 2 has more pressure and has a higher pressure difference between the wells than other heterogeneous cases. This is an interesting phenomenon because heterogeneous case 2 has similar average permeability as other heterogeneous cases (Table 1). To investigate this phenomenon, we filtered out low permeability cells of all realisations of heterogeneous case 2 and case 3 as shown in Fig. 9. It is evident from the figure that the impermeabilities in case 2 are more predominant than in case 3. Therefore, we can conclude that the distribution and variation of permeability affect CoP, even if the average permeability is the same between different domains.

Moving on to simulation case V, where we did the simulations of case IV for life time fixed at 30 years, the simulations for two heterogeneous cases 1 and 2 show that the optimal solutions shift to $L = dx = 600$ m as a

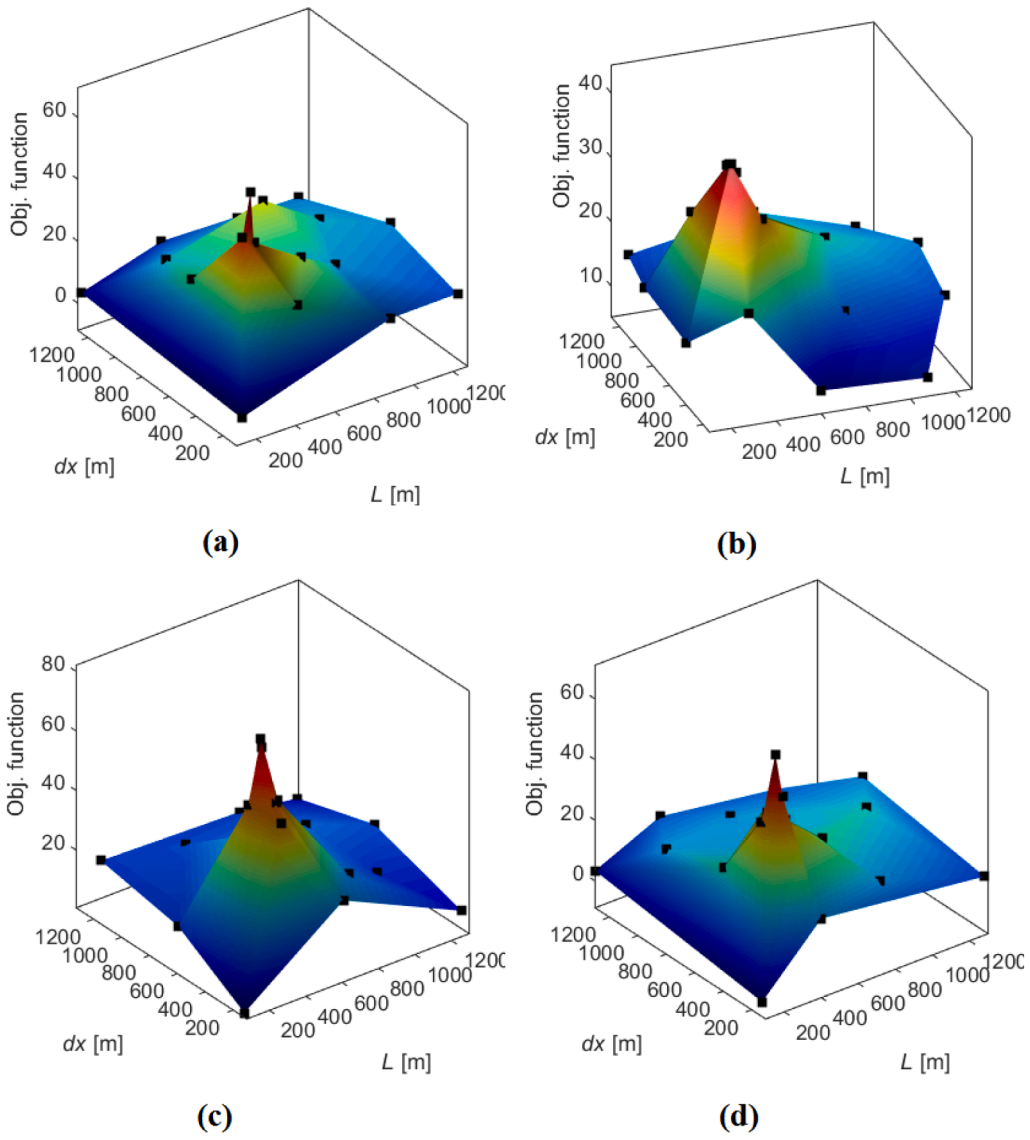

Fig. 14. Objective function surfaces for simulation cases XI (a to d for heterogeneous cases 1 to 4, respectively).

result of extending the life times as shown in Fig. 10(a and b). This is supported by Fig. 10(c and d) where the objective function values of simulation cases IV and V are compared. The trend of increase in optimal solution is affected by shift in $E_{in} - E_{out}$as shown in Fig. 10(e and f). These figures show $E_{in} - E_{out}$ optima occur at about $L = dx = 500$ m to 600 m as a result of an extended time (30 years compared with 15 years) to extract energy from the license region.

In terms of CoP, similar to Fig. 7, in Fig. 11 we show the results of conducting individual realisations-based simulations of case V. Heterogeneity case 1 has an optimal value of 700 m for CoP, heterogeneity case 2 shows a steady increase in CoP as the distances increase, heterogeneity case 3 has an optimal value of 700 m for CoP, and heterogeneity case 4 has an optimal value of 800 m for CoP. Therefore, except for heterogeneity case 1, the other cases have the same CoP trend vs. L and dx compared with simulation case IV.

4.3. Case VI (surrogate-assisted optimisation on 3D heterogeneous cases)

Our first set of surrogate-assisted optimisation, using the methodology briefly explained in Section 3.3, is simulation case VI. The profiles of sorted (from low to high) objective function values are presented in Fig. 12. We have sorted the values as the optimisation algorithm tries to construct the surfaces as shown in the subsets of Fig. 12 through candidate points, so the actual plots of objective function values with respect to function evaluation will be unsorted from low to high values. The optimal solutions obtained for $L$and $dx$for each heterogeneous case are reported in Table 4. We should note that due to significantly higher than 1 °C production temperature drop, the life time for most of the function evaluations will be 15 years. That is, the life time is restricted to not be lower than 15 years so that if a temperature drop of 1 °C happens earlier than 15 years, the simulation automatically chooses 15 years as the life time. There are only a few cases that the function evaluation lead to life times larger than 15 years. Therefore the results of optimisation for this simulation case should be compared with the results of simulation case IV in Table 3 and Fig. 6(e). It is clear that the optimisation algorithm has been mostly successful to locate the optimal points within only 20 function evaluations (compared with 100 for the simple-search format for simulations). Even for heterogeneous case 1, $L = dx = 425$ m obtained by optimisation has led to higher value for objective function than $L = dx = 400$ m obtained by simple-search format of simulations (38 compared with 34). This is the opposite for heterogeneous case 3. For heterogeneous case 4, the surrogate-based optimisation has converged to the second optimal peak (see Fig. 6(d) at $L = dx = 475$ m).

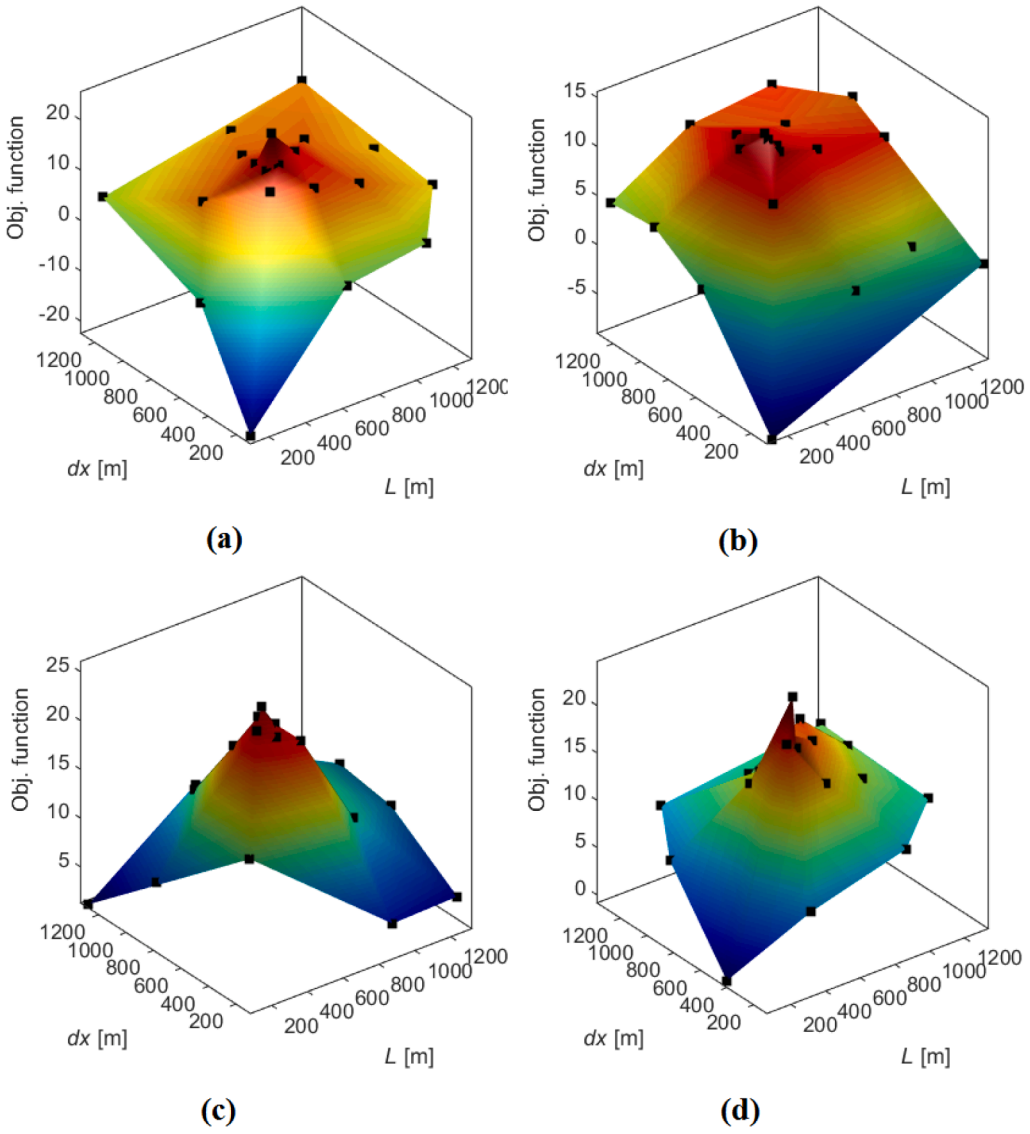

Fig. 15. Objective function surfaces for simulation cases XII (a to d for heterogeneous cases 1 to 4, respectively).

Table 5
Optimisation results for simulation cases XI and XII.

Simulation case	Heterogeneity case	Optimal L [m]	Optimal dx [m]	Optimal obj. function value
XI	1	325	325	61
XI	2	300	400	41
XI	3	325	325	82
XI	4	325	325	66
XII	1	575	575	24
XII	2	450	575	16
XII	3	475	525	26
XII	4	575	575	25

4.4. Cases VII, VIII, IX, and X (effects of discharge rate on 3D homogeneous cases)

These simulation cases are defined to investigate the effect of discharge rate on the optimal location and placement of doublets, as well as the outputs of optimisations and simulations. Fig. 13 shows the objective function, CoP, $E_{in} - E_{out}$ for simulation cases VII, VIII, IX, and X, compared with simulation cases I and II. The following can be deducted from the figure:

- The lower discharge rate of 150 m^3/hr (simulation cases VII and VIII) has increased the objective function values by increasing CoP (lowering pressure difference between injection and production wells) compared with simulation cases I and II,
- The higher discharge rate of 400 m^3/hr (simulation cases IX and X) has decreased the objective function values by decreasing CoP compared with simulation cases I and II,
- The lower discharge rate of simulation case VII has shifted the optimal L and $dx$to 300 m compared with simulation case I with optimal values of 400 m. Similarly, simulation case VIII has optimal values of L and $dx$for 100 m to 200 m lower than simulation case II. Therefore, decrease in discharge rate leads to decrease in optimal L and dx.
- The higher discharge rate of simulation case IX has shifted the optimal L and dx to 500 m compared with simulation case I with optimal values of 400 m. Similarly, simulation case X has optimal values of L and dx for 100 m higher than simulation case II (700 m compared with 600 m). Therefore, increase in discharge rate leads to increase in optimal L and dx.

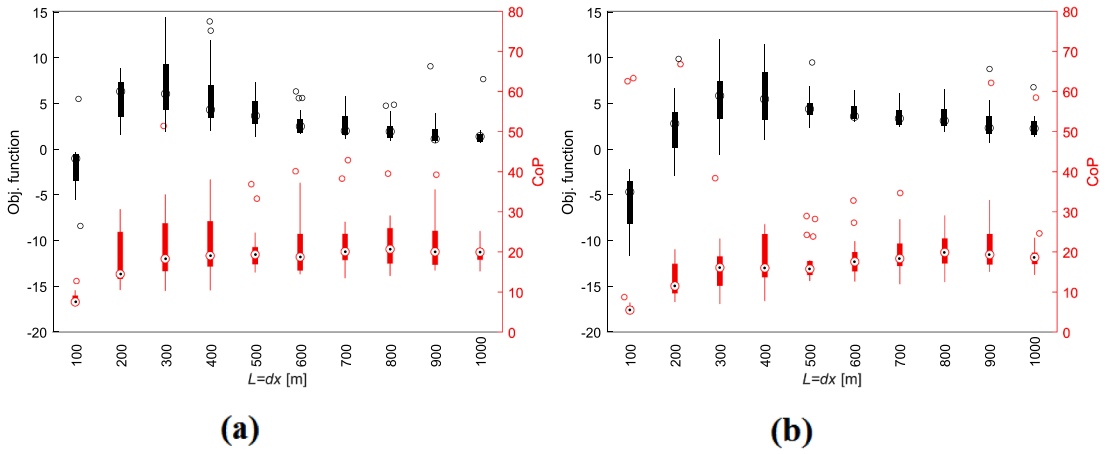

Fig. 16. Box plots of simulation results vs. $L = dx$ from case XIII and XIV with 20 realisations (objective function and CoP separately calculated for each realisation), for (a) case XIII, and (b) case XIV.

- $E_{in} - E_{out}$ shows the same trend of decrease in discharge rate leading to decrease in optimal L and dx, and increase in discharge rate leading to increase in optimal L and dx

4.5. Cases XI and XII (Effects of discharge rate on correlated heterogeneous cases using surrogate-assisted optimisation)

The results of the last two sets of simulations using the surrogate-based optimisation are presented here (Figs. 14 and 15). The optimal solutions obtained for L and dx for each heterogeneous case are reported in Table 5. When we compare L and dx of this table with those of Table 4 for surrogate-assisted optimisation of base case discharge rate, we can observe that on average the optimal values of L and dx have decreased by ~100 m by the lower discharge rate of 150 m^3/hr, and increased by ~100 m by the higher discharge rate of 400 m^3/hr.

It is interesting that some of the surfaces feature prominent spikes over the optimal location. This is because for such cases both components of the objective function ($E_{in} - E_{out}$ and CoP) are synchronously maximised at the optimal location. This shows that the objective function defined in our work can be used with confidence to optimise the performance of variously heterogeneous geothermal aquifers under different operating conditions (discharge rate and life time). The definition is robust against spatially correlated heterogeneity of various correlation lengths.

4.6. Cases XIII, XIV, XV, and XVI (Braided model: effects of channels in the 2D domain)

Using 20 realisations of 2D fluvial braided channels as shown in Fig. 2(h), simulation cases XIII and XIV are conducted. A major difference between this model with the 3D model in terms of process performance is the poorer injectivity of this model due to impermeabilities around the channels. Therefore, the target injection rate of 250 m^3/hr could not be achieved for some realisations throughout the operation life time. Despite these complexities, Fig. 16(a and b) for objective function and CoP vs. $L = dx = 100$ to 1000 m, show that the objective function is optimised again around 300 m to 400 m for LT = 15 years (simulation case XIII) and LT = 30 years (simulation case XIV), respectively. CoP, however, displays extreme variabilities for different simulations, but overall, due to the unfavourable permeability distribution and the pressure build-up in the domain, the values of CoP are lower than the 3D case. The trend of CoP vs. $L = dx =$ is positive until 900 m, but at 1000 m there is a decline in CoP, showing no strong optimality with respect to CoP values.

In Fig. 17, we showed the temperature distributions of 10 fluvial braided model realisations at life time of 15 years (simulation case XIII) for $L = dx = 100$ m (Fig. 17a), 400 m (Fig. 17 and 1000 m (Fig. 17c). Also, we have shown for each realisation, the licensed area (hashed cyan line), wells (blue and red circles), and values of E_{in} and E_{out} (white text). It is visually, as well as quantitatively, clear that $L = dx = 400$ m is producing the optimal coverage of the licensed area. If the well/doublet spacings are decreased, E_{out} increases, and if the well/doublet spacings are increased, E_{in} decreases. Either of these renders the heat recovery processes suboptimal in terms of the heat extraction efficiency from the licensed region.

Finally, Fig. 18 shows the results of simulation case XV and simulation case XVI. The following points are observed about these figures. Firstly, the ranges of variations (the size of the bars in box plots) of the objective function and CoP for case XV are larger than those for case XVI. This is due to the orientation of braided channels that are in the I1-I2 orientation for case XV and are in the P1-P2 orientation for case XVI. Therefore, for case XV depending on whether the line connecting I1 and I2 is inside or outside the channels, the results of the simulations vary rather significantly. If the I1-I2 line is inside the channels, the injected cold water is diverted from production wells. Also, in this case, the pressure difference between the wells remains low, and as such CoP is higher compared with case XVI. This happens more emphatically for $L = dx = 100$ m. Therefore, while for case XV the maximum CoP happens at for $L = dx = 100$ m, for case XVI, $L = dx = 900$ m is optimal for CoP. Higher CoP of case XV leads to higher objective functions as well compared with case XVI. However, the optimal well/doublet spacing for both cases again happens at 300 m to 400 m.

5. Conclusions and future works

Using a series of homogeneous and uncertain heterogeneous (with spatial correlation in porosity/permeability and channelised porosity/permeability) porous media, we investigated the optimal locations of wells and doublet spacing. We defined a novel objective function that maximises heat recovery from the licence region, minimises heat recovery from outside of the license region, and maximises the Coefficient of Performance. Our results showed:

- Based on a fixed life time of 15 years, we found that the optimal well/doublet spacing of checkerboard pattern is 400 m for the discharge rate of 250 m^3/day. This spacing consistently produces optimal values for the objective functions for homogeneous and heterogeneous cases.
- The optimal solution comprising the multiplication of "Coefficient of Performance" into "heat recovery from the license region minus heat recovery from outside the license region", can be predominantly optimal for the heterogeneous cases with low discharge rate where

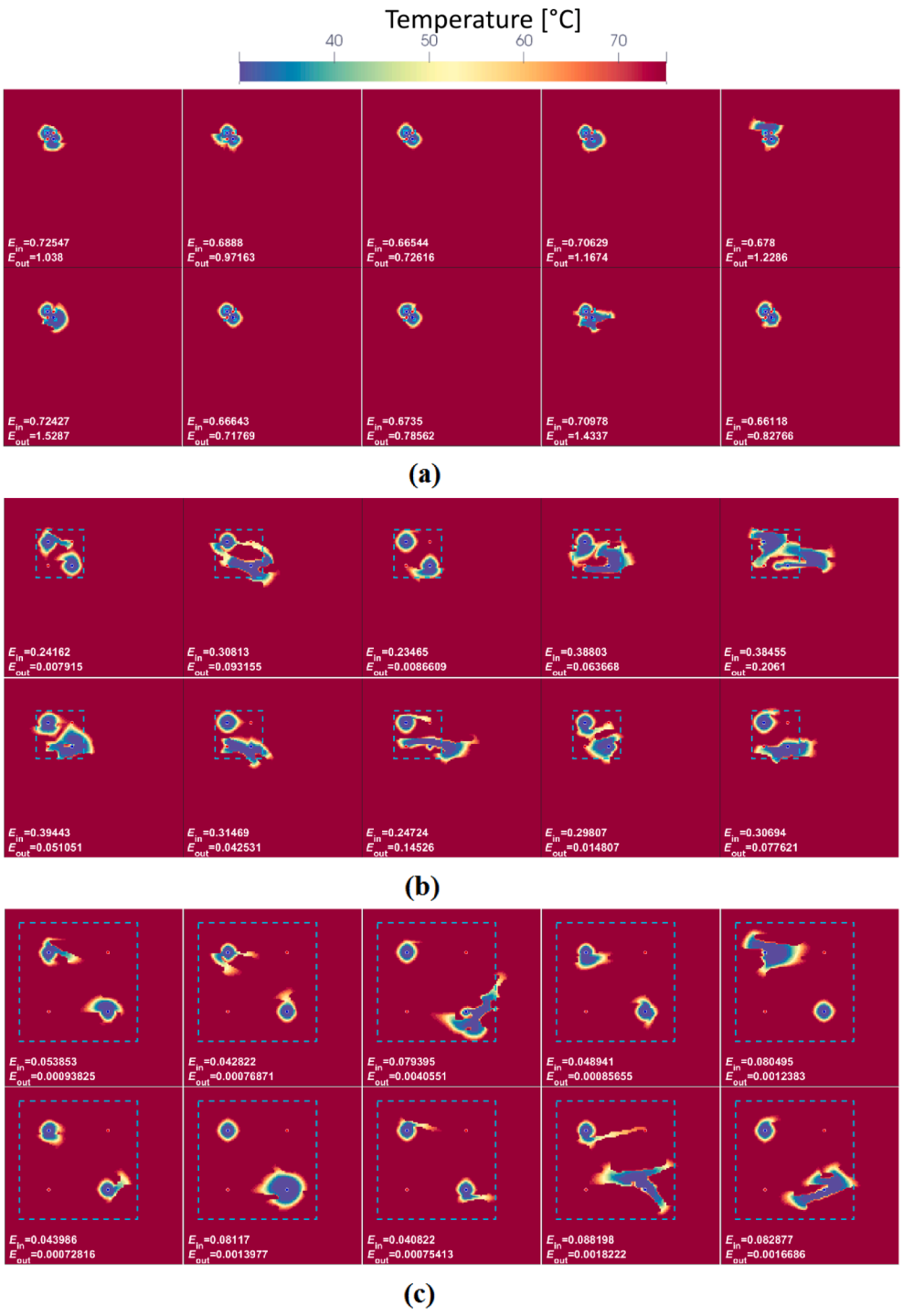

Fig. 17. Temperature profile at life time of 15 years for 10 realisations of braided model in y-direction for (a) $L = dx = 100$ m, (b) $L = dx = 400$ m, and (c) $L = dx = 1000$ m.

both components of the objective function are synchronously optimised at the optimal solution.

- Increase in life time will lead to a higher optimal spacing of 600 m for the homogeneous case and heterogeneous cases for the discharge rate of 250 m^3/day.
- Increase in rate also increases the optimal well location and spacing.
- Surrogate response surfaces are successfully used to obtain the optimal solutions in a computationally efficient way (20 simulations compared with 100 simulations without the surrogate-based optimisation algorithm).
- The distribution of permeability and in particular the correlated heterogeneity clusters affect the values of CoP (more than the objective function defined in this work). Therefore, the mean and standard deviation of permeability alone cannot be considered as the sole parameters to determine the performance of heat recovery from geothermal sources. Our results show that for complex heterogeneous media, 700 m to 900 m produce relatively the best CoPs for various cases of heterogeneity in porosity and permeability.

Our future studies will include multiple patterns of wells (not just checkerboard), addition of CO_2, and geochemical interaction of working

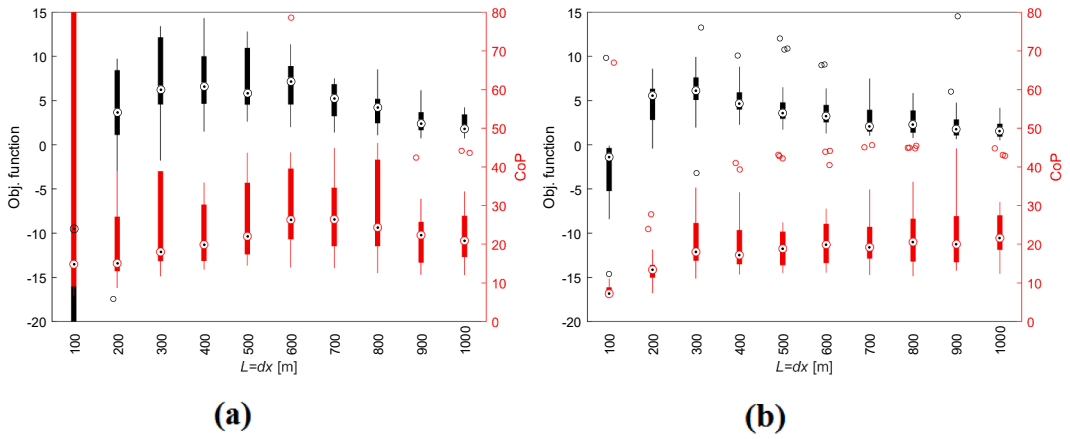

Fig. 18. Box plots of simulation results vs. $L = dx$ from case XV and XVI with 20 realisations (objective function and CoP separately calculated for each realisation), for (a) case XV, and (b) case XVI.

fluid and rock into the optimisation processes. Moreover, we assumed rock density, heat capacity ad thermal conductivity as homogeneous, whereas in reality, these properties are also heterogeneous.

Also, the fractured networks models can be incorporated into the existing model to investigate the effects of fractures on optimal well/doublet spacing. In this work, we only had two state variables of *dx* and *L*. Many other operational variables can be added if we consider multiple doublets and various well patterns in heat extraction. Also, as a result of varying the patterns, the definition of license area will have to be updated or impacts of its conventional definitions on heat recovery, CoP, and Energy Sweep should be tested,

CRediT authorship contribution statement

Masoud Babaei: Conceptualization, Methodology, Formal-analysis, Software, Writing-review-editing. **Amir Mohammad Norouzi:** Methodology, Writing-review-editing. **Hamidreza M. Nick:** Conceptualization. **Jon Gluyas:** Conceptualization.

Declaration of Competing Interest

The authors declare that they have no known competing financial interests or personal relationships that could have appeared to influence the work reported in this paper.

Acknowledgment

MB would like to acknowledge the support received from the University of Manchester to provide a HP Proliant Server on which the simulations were carried out.

References

[1] Schulte DO, Arnold D, Geiger S, Demyanov V, Sass I. Multi-objective optimization under uncertainty of geothermal reservoirs using experimental design-based proxy models. Geothermics 2020;86:101792.
[2] Blank L, Rioseco EM, Caiazzo A, Wilbrandt U. Modeling, simulation, and optimization of geothermal energy production from hot sedimentary aquifers. Comput Geosci 2021;25(1):67–104.
[3] Pandey S, Vishal V, Chaudhuri A. Geothermal reservoir modeling in coupled thermo-hydro-mechanical-chemical approach: a review. Earth-Sci Rev.
[4] Sauty J, Gringarten A, Landel P, Menjoz A. Lifetime optimization of low enthalpy geothermal doublets. In: Advances in European geothermal research. Springer; 1980. P. 706–719.
[5] Tselepidou K, Katsifarakis K. Optimization of the exploitation system of a low enthalpy geothermal aquifer with zones of different transmissivities and temperatures. Renew Energy 2010;35(7):1408–13.
[6] Smit R, Salimi H, Wolf K. Optimization of geothermal-well-doublet placement. In: 76th EAGE conference and exhibition 2014; 2014.
[7] Ansari E, Hughes R, White CD. Well placement optimization for maximum energy recovery from hot saline aquifers. In: 39th Workshop on geothermal reservoir engineering, SGP-TR-202. Stanford: Stanford University; 2014.
[8] Kong Y, Pang Z, Shao H, Kolditz O. Optimization of well-doublet placement in geothermal reservoirs using numerical simulation and economic analysis. Environ Earth Sci 2017;76(3):118.
[9] Jiang Z, Xu T, Wang Y. Enhancing heat production by managing heat and water flow in confined geothermal aquifers. Renew Energy 2019;142:684–94.
[10] Willems CJ, Nick H. Towards optimisation of geothermal heat recovery: an example from the west Netherlands basin. Appl Energy 2019;247:582–93.
[11] Liu G, Wang G, Zhao Z, Ma F. A new well pattern of cluster-layout for deep geothermal reservoirs: case study from the Dezhou geothermal field, China. Renew Energy 2020;155:484–99.
[12] Gadd C, Xing W, Nezhad MM, Shah A. A surrogate modelling approach based on nonlinear dimension reduction for uncertainty quantification in groundwater flow models. Transp Porous Media 2019;126(1):39–77.
[13] Vogt C, Mottaghy D, Wolf A, Rath V, Pechnig R, Clauser C. Reducing temperature uncertainties by stochastic geothermal reservoir modelling. Geophys J Int 2010;181(1):321–33.
[14] Chen M, Tompson AF, Mellors RJ, Abdalla O. An efficient optimization of well placement and control for a geothermal prospect under geological uncertainty. Appl Energy 2015;137:352–63.
[15] Ansari E, Hughes R. Response surface method for assessing energy production from geopressured geothermal reservoirs. Geotherm Energy 2016;4(1):15.
[16] Asai P, Panja P, McLennan J, Moore J. Performance evaluation of enhanced geothermal system (EGS): surrogate models, sensitivity study and ranking key parameters. Renew Energy 2018;122:184–95.
[17] Pollack A, Mukerji T. Accounting for subsurface uncertainty in enhanced geothermal systems to make more robust techno-economic decisions. Appl Energy 2019;254:113666.
[18] Willems CJ, Nick HM, Weltje GJ, Bruhn DF. An evaluation of interferences in heat production from low enthalpy geothermal doublets systems. Energy 2017;135:500–12.
[19] Babaei M, Nick H. Performance of low-enthalpy geothermal systems: interplay of spatially correlated heterogeneity and well-doublet spacings. Appl Energy.
[20] Cirpka OA. Generation of random, autocorrelated, periodic fields [online]; 2003.
[21] TNO. TNO Nl olie- en gasportaal [online]; 1977.
[22] Sutter A. Sedimentology, depositional environments and sequence stratigraphy [online]; 2008.
[23] Fritsch FN, Carlson RE. Monotone piecewise cubic interpolation. SIAM J Numer Anal 1980;17(2):238–46.
[24] Incropera FP, Lavine AS, Bergman TL, DeWitt DP. Fundamentals of heat and mass transfer. Wiley; 2007.
[25] Schlumberger, ECLIPSE Technical Description 2014.1; 2014.
[26] Willems CJ, Nick H, Goense T, Bruhn D. The impact of reduction of doublet well spacing on the net present value and the life time of fluvial hot sedimentary aquifer doublets. Geothermics 2017;68:54–66.
[27] Müller J. Surrogate model optimization toolbox. Tech. rep., Tampere University of Technology; 2012.
[28] Babaei M, Pan I. Performance comparison of several response surface surrogate models and ensemble methods for water injection optimization under uncertainty. Comput Geosci 2016;91:19–32.
[29] Babaei M, Alkhatib A, Pan I. Robust optimization of subsurface flow using polynomial chaos and response surface surrogates. Comput Geosci 2015;19(5):979–98.
[30] Müller J, Piché R. Mixture surrogate models based on Dempster-Shafer theory for global optimization problems. J Global Optim 2011;51(1):79–104.
[31] Regis RG, Shoemaker CA. A stochastic radial basis function method for the global optimization of expensive functions. INFORMS J Comput 2007;19(4):497–509.
[32] DoE, Guide to Geothermal Heat Pumps. URL:https://www.energy.gov/sites/prod/files/guide_to_geothermal_heat_pumps.pdf.